ACS APPLIED MATERIALS & INTERFACES

Research Article

www.acsami.org

Electrochemically Active Nickel Foams as Support Materials for Nanoscopic Platinum Electrocatalysts

Julia van Drunen,[†] Brandy K. Pilapil,[‡] Yoseif Makonnen,[†] Diane Beauchemin,[†] Byron D. Gates,[‡] and Gregory Jerkiewicz*,[†]

[†]Department of Chemistry, Queen's University, 90 Bader Lane, Kingston Ontario K7L 3N6, Canada

[‡]Department of Chemistry and 4D LABS, Simon Fraser University, 8888 University Drive, Burnaby British Columbia V5A 1S6, Canada

Supporting Information

ABSTRACT: Platinum is deposited on open-cell nickel foam in low loading amounts via chemical reduction of Pt cations (specifically, Pt^{2+} or Pt^{4+}) originating from aqueous Pt salt solutions. The resulting Pt-modified nickel foams (Pt/Ni foams) are characterized using complementary electrochemical and materials analysis techniques. These include electron microscopy to examine the morphology of the deposited material, cyclic voltammetry to evaluate the electrochemical surface area of the deposited Pt, and inductively coupled plasma optical emission spectrometry to determine the mass of deposited Pt on the Ni foam substrate. The effect of potential cycling in alkaline media on the electrochemical behavior of the material and the stability of Pt deposit is studied. In the second part of this paper, the Pt/Ni foams are applied as electrode materials for hydrogen evolution, hydrogen reduction, oxygen reduction, and oxygen evolution reactions in an aqueous alkaline electrolyte. The electrocatalytic activity of the electrodes toward these processes is evaluated using linear sweep voltammetry curves and Tafel plots. The results of these studies demonstrate that nickel foams are acceptable support materials for nanoscopic Pt electrocatalysts and that the resulting Pt/Ni foams are excellent electrocatalysts for the hydrogen evolution reaction. An unmodified Ni foam is shown to be a highly active electrode for the oxygen evolution reaction.

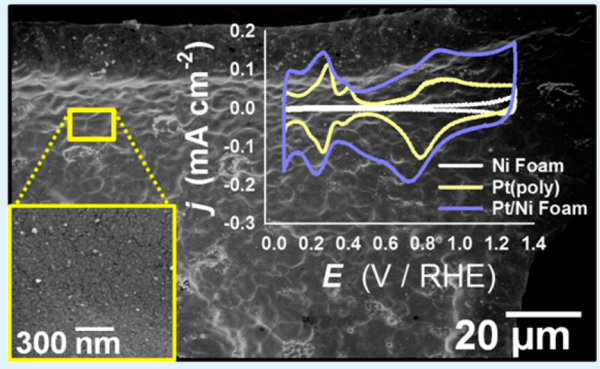

KEYWORDS: *alkaline water electrolysis, nickel electrocatalyst, platinum electocatalyst, nickel foam, three-dimensional electrode*

INTRODUCTION

The following four electrochemical reactions presented for an alkaline aqueous electrolyte are of upmost importance to water electrolysis and hydrogen fuel cell technologies: (i) hydrogen evolution reaction (HER, eq 1); (ii) hydrogen oxidation reaction (HOR, eq 2); (iii) oxygen reduction reaction (ORR, eq 3); and (iv) oxygen evolution reaction (OER, eq 4).

$$2H_2O + 2e^- \rightarrow H_2 + 2OH^- \quad (1)$$

$$H_2 + 2OH^- \rightarrow 2H_2O + 2e^- \quad (2)$$

$$O_2 + 2H_2O + 4e^- \rightarrow 4OH^- \quad (3)$$

$$4OH^- \rightarrow O_2 + 2H_2O + 4e^- \quad (4)$$

The availability of high-purity hydrogen gas (H_2 (g)) is one important challenge that must be addressed in order for fuel cells to be considered viable energy-delivering technologies. The global demand for H_2 (g) grows at a rate of approximately 10% per year and is driven by its use in fertilizer production, food processing, and metallurgical applications.[1,2] Increased commercialization of hydrogen fuel cells will contribute to the growing demand for high-purity H_2 (g) that is generated through a limited number of processes including water electrolysis (eq 5 presents the overall reaction).[2,3] It is generally accepted that the mechanism of cathodic HER occurring at a solid metallic electrocatalyst (M (s)) proceeds through the steps outlined in eqs 6−8.[4−10]

$$H_2O(l) \rightarrow H_2(g) + \frac{1}{2}O_2(g) \quad (5)$$

$$M(s) + H_2O(l) + e^- \rightarrow M - H_{OPD} + OH^-(aq) \quad (6)$$

$$M - H_{OPD} + H_2O(l) + e^- \rightarrow M(s) + H_2(g) + OH^-(aq) \quad (7)$$

$$2M(s) - H_{OPD} \rightarrow 2M(s) + H_2(g) \quad (8)$$

where H_{OPD} refers to the overpotential deposited H that is a reaction intermediate. Many commercial alkaline electrolyzers use Ni-based electrodes due to their stability in alkaline

Received: February 21, 2014
Accepted: July 16, 2014
Published: July 16, 2014

media,[11,12] the electrocatalytic activity of Ni,[11,13] and the relatively low cost of Ni-based materials. A large number of studies are available examining water electrolysis using electrodes comprised of combinations of Ni and other metals, such as Ni/Fe,[14−16] Ni−Zn,[7,15] Ni−Fe−Zn,[15] Ni−P,[17] Co−P,[17] Ni−P−Fe,[17] Ni−Mo,[15,18] Ni−Mo−Cd,[18] Ni/NiFeS,[19] Raney-Ni/Mo,[10] Ni/spinel-type Co_3O_4, Ni/La-doped Co_3O_4,[20] and others. The development of industrial electrode materials focuses on low-cost, high efficiency, and long lifetime; in this respect, Ni-based materials are relevant electrocatalysts for alkaline water electrolysis. Several types of fuel cells operate in alkaline conditions and utilize Pt or combined Pt/Ni electrocatalysts for HOR or ORR.[21−26] The results presented herein are applicable to the development of water electrolyzers, alkaline fuel cells, and alkaline alcohol fuel cells.

Open-cell metallic foams are of interest for research in electrochemistry due to their rigid, open porous network, which affords these materials a large surface area for electrochemical utilization and can allow for good mass-transport properties.[27] A number of studies describe the use of Ni-based foams as an electrode support material for other electrocatalysts including Pt,[28−30] Rh,[29,31] Pd,[32−34] Ag,[35] Sn−Co,[36] and Co−W−B.[37] As an electrocatalyst support material, Ni foams offer valuable structural characteristics including a consistent open-pore three-dimensional structure with tunable density and large surface area, and good stability in a range of different electrolytes, including strongly alkaline conditions.[38] Because of the electrocatalytic activity of Ni toward a variety of reactions that include the HER and OER, the Ni foam can act as both an electrocatalyst in itself and as a Pt electrocatalyst support material.

This study presents the fabrication and characterization of Pt/Ni foams using a combination of materials science, electrochemical, and analytical techniques. The Pt/Ni foam electrodes are evaluated in terms of their stability in an aqueous alkaline environment and their electrocatalytic activity toward the four above-mentioned reactions. Scanning electron microscopy (SEM) is used to examine the size and morphology of the deposited Pt particles; energy-dispersive X-ray spectroscopy (EDS) during electron microscopy analysis is used to verify the presence of Pt particles on the Ni foam surfaces; cyclic voltammetry (CV) is used to determine the electrochemically active surface area (A_{ecsa}) of the deposited Pt; and mass of the deposited Pt is determined by inductively coupled plasma optical emission spectrometry (ICP-OES). Each of the aforementioned electrochemical reactions, namely, HER, HOR, ORR, and OER, are conducted in alkaline media using Pt-modified Ni foams with various Pt mass loadings, as well as unmodified Ni foam and polycrystalline Pt (Pt(poly)). These electrochemical reactions are studied using linear sweep voltammetry (LSV) and steady-state polarization curves (Tafel plots).

EXPERIMENTAL SECTION

Preparation of Pt/Ni Foams. Deposition of Pt on Ni foam was accomplished using an electroless deposition method that is similar to the impregnation method described elsewhere.[39−43] The Ni foam used in these studies was supplied by the former Inco Technical Services Ltd. Uniform Ni foam disks (bulk density ρ = 0.21 g cm^{-3}), having diameters equal to 10 mm and being ca. 3 mm in thickness, were first prepared using a stainless steel punch. Extensive structural, chemical, electrochemical, and morphological characterization of the Ni foam used in this study and other similar Ni foam materials is available elsewhere.[44,45] Prior to the deposition of Pt, each Ni foam disk was degreased with acetone under reflux for 2 h to remove any organic impurities. The foam was then dried in ultrahigh purity (UHP) N_2 (g) atmosphere and weighed using an analytical balance. To deposit Pt, the Ni foam disk was first placed in a glass vial and submerged in 10 mL of 0.20 M aqueous $NaBH_4$ (a chemical reducing agent) for 120 s, allowing the pores of the foam to become saturated with the solution. The foam was then removed from the $NaBH_4$ solution and, while still wetted with the $NaBH_4$ solution, placed in a glass vial with 10 mL of an aqueous solution of Pt salt and allowed to soak for 120 s. Four different Pt salt solutions consisting of two Pt salts with different Pt oxidation states (Pt^{2+} and Pt^{4+}) and two concentrations for each oxidation state were applied. Thus, the deposition solutions were as follows: 1 mM K_2PtCl_4 (type A), 2 mM K_2PtCl_4 (type AA), 1 mM K_2PtCl_6, (type B), and 2 mM K_2PtCl_6 (type BB). All solutions contained 0.10 M KOH, in addition to the dissolved Pt salt. After soaking for 120 s in the Pt salt solution, the foam was placed in fresh $NaBH_4$ for an additional 120 s and then again in fresh Pt salt solution for 120 s. The deposition steps were repeated 2, 5, or 10 times, as indicated by the number of times the Ni foam was soaked in the Pt salt solution. The nomenclature used herein refers to the concentration and type of Pt salt in the deposition solution, as well as the number of depositions. For example, samples of type AA10 are prepared using 2 mM K_2PtCl_4 solution with 10 deposition events. The final deposition step was always submersion in the $NaBH_4$ solution. Rinsing and sonicating in UHP water was used to remove deposition solution that could be trapped within the Ni foam pores before drying the electrodes in a stream of UHP N_2 (g). All aqueous solutions were made with UHP water (Millipore).

Electrochemical Measurements. Electrochemical measurements were carried out using a two-compartment Pyrex electrochemical cell and three electrodes. The working electrode (WE) was either an unmodified Ni foam disk, a Pt(poly) wire, or a Pt/Ni foam disk prepared using the method described above. The foam materials were attached to a thin Ni wire (Alfa Aesar Puratronic, 0.25 mm in diameter) by winding it through the mesh; the Ni wire was sealed in a glass tube, and the quality of the electrical connection was verified by examining the electrical resistance that was practically zero. The contribution of the Ni wire to the overall surface area in contact with the electrolyte, and thus to the electrochemical signal, is less than 1% and is assumed to be negligible.[44,45] The counter electrode (CE) consisted of high-purity Pt gauze (99.98% in purity, Alfa Aesar) spot-welded to a Pt wire (99.98% in purity, Alfa Aesar) and covered with electrodeposited Pt (Pt black). The surface area of the CE was at least 10 times larger than that of the WE. The separation between WE and CE was approximately 3 cm. The reference electrode (RE) was a reversible hydrogen electrode (RHE) made in the same manner as the CE. Hydrogen gas (UHP, Praxair 5.0 grade) was bubbled through the RE compartment at a pressure of 1 bar. All potentials herein are reported with respect to RHE. The RE was in electrolytic contact with WE via a Luggin capillary to minimize the uncompensated resistance of the solution (the so-called IR drop). Electrochemical characterization was carried out in 0.50 M aqueous KOH solution (Sigma-Aldrich KOH pellets, A.C.S. reagent grade) prepared using UHP water. Prior to each experiment, the electrolyte solution was degassed by bubbling UHP N_2 (g) (Praxair 5.0 grade) for 30 min. Throughout the duration of electrochemical measurements, UHP N_2 (g) was passed over the electrolyte to maintain an inert gas environment. Electrochemical impedance spectroscopy (EIS) was used to determine the value of IR for this electrochemical set up at various potential values (i.e., E = −0.20, 0.00, 0.20, 0.80, and 1.50 V). The value of IR = 0.68 ± 0.04 Ω was determined by taking an average value of four separate measurements at each of the potentials mentioned (a total of 20 measurements). Glassware was cleaned according to well-established procedures.[46] The electrochemical measurements were carried out at a temperature of T = 298 ± 1 K. An Autolab model PGSTAT302 potentiostat (Metrohm) equipped with NOVA Advanced Electrochemical Software (Metrohm) was used to control experimental parameters and to acquire the data.

The following four reactions were carried out using unmodified Ni foam, Pt(poly), and Pt/Ni foam electrodes: (i) HER; (ii) HOR; (iii) ORR; and (iv) OER. Each reaction was carried out using two different experimental methods, namely, linear sweep voltammetry (LSV) and a

staircase-type Tafel polarization program. The Tafel polarization experiments were performed by preprogramming the potentiostat to apply a sequence of potential (E) steps, each with a magnitude of 5 mV. Each E value was maintained for 10 s, and during this time the current (I) was recorded. At each E, the value of I was determined by averaging it for the last 2 s of the I versus time transient; such determined I value represents near steady-state conditions. The 0.50 M aqueous KOH electrolyte was purged with N_2 gas for 60 min then saturated with either H_2 (g) (in the case of HER and HOR) or O_2 (g) (in the case of ORR and OER) by bubbling the gas through the electrolyte for 30 min while stirring. Throughout the electrochemical measurements, the electrolyte was stirred, and H_2 (g) or O_2 (g) was passed above the electrolyte to maintain saturation. The history of the electrode has an important influence on its electrochemical behavior.[47] Both Ni and Pt form oxides in E ranges that overlap with the ORR and OER; the presence of an oxide can influence the material's electrocatalytic activity. In an effort to control the history of the Pt/Ni foam electrodes, the LSV and Tafel polarization measurements were always performed in the following sequential order:

1. Electrolyte purging for 60 min with N_2 (g);
2. Potential scanning (CV) 100 times in the $0.005 \leq E \leq 1.30$ V range at $s = 100$ mV s^{-1} with N_2 (g) purging;
3. Electrolyte saturation with H_2 (g) for 30 min;
4. HER LSV experiment followed by HER Tafel polarization experiment;
5. HOR LSV experiment followed by HOR Tafel polarization experiment;
6. Electrolyte purging with N_2 (g) for 60 min;
7. Potential scanning (CV) 100 times in the $0.005 \leq E \leq 1.30$ V range at $s = 100$ mV s^{-1} with N_2 (g) purging;
8. Electrolyte saturation with O_2 (g) for 30 min;
9. ORR LSV experiment followed by ORR Tafel polarization experiment; and
10. OER LSV experiment followed by OER Tafel polarization experiment.

Further details pertaining to the LSV and Tafel polarization measurements are provided in the Supporting Information file.

Electron and Ion Microscopy. Complementary electron- and ion-imaging techniques were used to analyze the Pt deposited on Ni foams. Scanning electron microscopy (SEM) characterization was performed using a Strata DB235 FESEM/FIB instrument equipped with an energy dispersive spectrometer (EDS) for elemental analysis (manufactured by EDAX) and operated at 5 kV. Focused gallium ion beam (FIB) analysis was performed using a Micrion 2500 instrument (FEI Company). The FIB instrument was used to acquire images in the secondary ion (SI) and secondary electron (SE) detection modes, which provide different topographical and chemical information.

Inductively Coupled Plasma Optical Emission Spectrometry Quantification of Platinum. Liquid samples for ICP-OES quantification of Pt on Ni foams were prepared through the following steps: (i) Pt/Ni foam disks (three of each type) were weighed using an analytical balance; (ii) each disk was digested in 2.0 mL of aqua regia (mixture of HCl and HNO_3 in 3:1 proportion by volume; the solution should be treated with caution as described in a respective Materials Safety Data Sheet) and sonicated for 30 min; (iii) the samples were diluted with 5 mL of UHP water. Sample blanks were prepared from unmodified Ni foam disks using the same method. The ICP-OES analysis was performed on the same day as the sample digestion. The analysis was performed using a lateral view ARCOS ICP-OES instrument (SPECTRO Analytical Instruments, Kleve, Germany) fitted with a concentric nebulizer (Glass Expansion, Victoria, Australia) and a cyclonic spray chamber (SCP Science, Quebec, Canada). Platinum and nickel standard solutions (0.1−500 mg L^{-1}) in ultrapure 2% (v/v) HNO_3 with 2% (v/v) HCl were prepared from commercially available 1000 mg L^{-1} single element standard solutions (SCP Science, Quebec, Canada) and UHP water. Optimization of the nebulizer gas flow rate was performed to arrive at a set of conditions that maximizes sensitivity for the Pt(II) 214.423 nm emission line. The optimized conditions are outlined in the Supporting Information file. The intensities of the Pt(II) 214.423 nm and Ni(II) 221.648 nm optical emission lines were analyzed. The standard solutions were aspirated in order of increasing concentration, followed by the aspiration of sample blanks, and then the samples to be analyzed. The optical emission intensities were blank-subtracted, and the elemental concentrations were determined by linear interpolation, using external calibration standards. The limits of detection for Pt and Ni were determined to be 0.04 and 0.01 μg L^{-1}, respectively. The limit of detection for Pt was at least 50 times lower than the amount of Pt in the least-abundant sample. Three samples of each type (A2, A5, A10, B2, B5, B10, AA2, AA5, AA10, BB2, BB5, BB10) were each analyzed in triplicates.

RESULTS AND DISCUSSION

Part 1: Characterization of Pt/Ni Foams. This section presents the characterization of Pt/Ni foams with respect to size and morphology of the deposited Pt particles, as well as the electrochemical properties of the resulting Pt/Ni materials. The amount of Pt deposited on the Ni foam is quantified with respect to the A_{ecsa} of Pt and the mass of deposited Pt per gram of Ni foam substrate.

Characterization of Pt/Ni Foams Using Scanning Electron Microscopy. Figure 1 displays one image of unmodified Ni foam and three SEM images of Pt/Ni foam at various levels of magnification. The Pt/Ni foam shown in these images is of the type AA 10, meaning that the Pt was deposited from 0.002 M K_2PtCl_4 solution with 10 deposition events. As discussed below, the AA 10 samples have the highest mass loading and highest surface area of Pt.

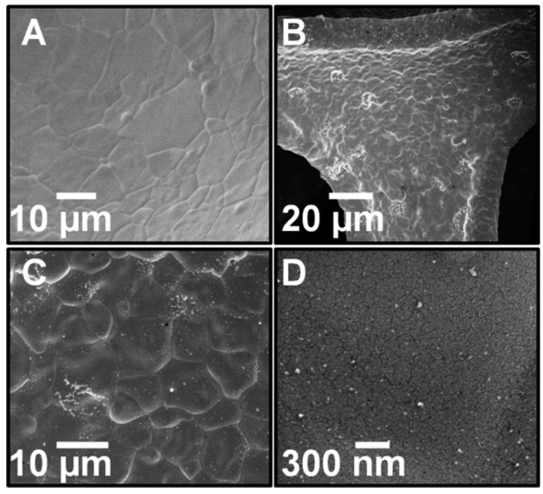

Figure 1. Secondary-electron scanning electron microscope image of unmodified Ni foam at 5000× magnification (A) and of Pt/Ni foam (type AA 10) at various levels of magnification, namely, 2540× (B), 10 000× (C), and 150 000× (D).

Focused ion beam secondary ion (FIB SI) images of each sample type were also collected and are shown for reference in the Supporting Information file. Image A of Figure 1 shows the surface microstructure of unmodified Ni foam; the surface is smooth with visible grain boundaries.[45] Image B shows Pt/Ni foam at a magnification of 2540×; at this level of magnification, the entire width of the strut that comprises the Ni foam structure is visible, and Pt particles can be seen dispersed over the surface. Image C shows Pt/Ni foam at a magnification of 10 000×; at this magnification, well-dispersed Pt particles are visible as small, bright specks. Some regions of the surface have clusters of small Pt particles concentrated in an ca. 1 μm

diameter area. Image D shows Pt/Ni foam at 150 000× magnification. The diameter of the deposited Pt particles is estimated to be in the 5−30 nm range. However, it is possible that higher magnification images would reveal the presence of smaller particles that cannot be observed at this scale. The Pt particle diameter was determined through the analysis of SEM images at the 150 000× and 200 000× level of magnification (see the figure and histogram in Supporting Information). The limited resolution of our SEM images likely skews this particle size analysis to be larger than the real value since only particles with a diameter greater than 5 nm could be quantified. For this reason we can only provide an estimate corresponding to the range of particle sizes. Other Pt/Ni foam samples were also analyzed by SEM and were found to have a similar size range of Pt deposits from 5−30 nm in diameter. Histogram analysis was not performed for all samples since it calculates only a skewed average due to the limited resolution. Further analysis by transmission electron microscopy could help to elucidate the particle size and distribution; however, we believe that this particular analysis is not necessary to evaluate the utility of Ni foams as a support material for Pt electrocatalysts.

The Ni foams used in this study have a consistent three-dimensional structure made up of struts that are 20−40 μm in width and interconnecting pores that are 300−500 μm across. The foams are manufactured in sheets that are ca. 3 mm in thickness, and a cross-section of the material reveals five to six layers of Ni struts through the depth of the foam (see the Supporting Information). The struts in the center of the foam are up to three layers away from the outer face of the material. In experiments that are not described within this contribution, we explored a variety of methods and conditions for depositing Pt on open-cell Ni foams and have encountered some difficulty with obtaining an even distribution of Pt throughout the depth of the material. Electrochemical deposition methods, for example, are particularly susceptible to the development of an uneven Pt deposition gradient from outer surfaces of the material to inner regions. The method described herein does not encounter these difficulties; rather, it produces an even distribution of Pt particles throughout the Ni foam structure. This was verified using the FIB instrumentation; FIB images that were collected at a variety of sample depths can be found in the Supporting Information section for this manuscript.[48]

Energy dispersive X-ray spectroscopy (EDS) was applied to confirm the presence of Pt on the Pt/Ni foams. Figure 2 shows

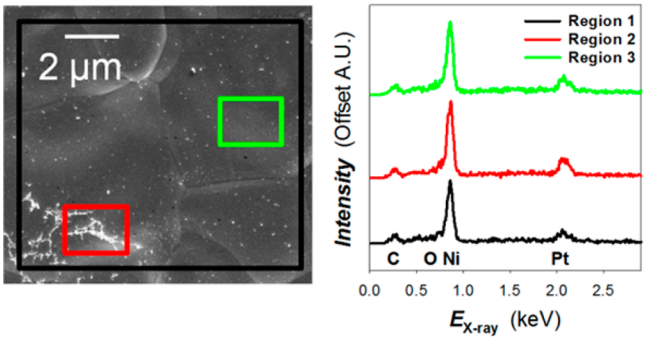

Figure 2. Energy dispersive X-ray spectroscopy (EDS) analysis performed at three regions on Pt/Ni foam (type AA 10). The three analysis regions are specified in the scanning electron microscope image on the left using colored boxes that are matched with corresponding EDS spectra.

EDS spectra collected from a Pt/Ni foam (type AA 10) at three regions that appear to have different amounts of Pt according to the corresponding SEM image on the left. The black, red, and green colored boxes on the SEM image correspond to the EDS spectra of matching color. The largest analysis area is ca. 36 μm^2 (Region 1, the large black rectangle). This region is meant to serve as a representative of the overall distribution of Pt over the surface. Region 1 has some locations with deposited Pt that are clustered together and other locations where only small Pt particles or no Pt particles are observed. Region 2 (the red rectangle) corresponds to an area of about 3 μm^2 that contains a cluster of deposited Pt on the surface. Region 3 (the green rectangle) corresponds to an area of about 3 μm^2 that, from the SEM image, does not appear to have very much Pt, and only a few small particles are visible. In each region Ni, Pt, C, and O are detected in the EDS analysis. The C and O are present as adsorbed surface species (CO_2) and metal oxides (β-Ni$(OH)_2$); carbon is a typical surface contaminant. Other than the peak corresponding to Pt, the EDS spectra for Regions 1, 2, and 3 are identical to the EDS spectra of an unmodified Ni foam.[45] The EDS spectra of the three regions displayed in Figure 2 are very similar to each other. In each region, the presence of Ni, C, O, and Pt is detected; Ni is the most abundant element in each spectrum. The peaks corresponding to C and O have similar intensities and shapes in the three spectra. The Pt peak in the EDS spectra is comparable in height and size, even though Pt appears to be more abundant in Region 2 as compared to Region 3 from the SEM image. Although this analysis is not quantitative, the observation that the Pt signal from Region 3 is comparable to that from Region 2 supports the proposal that the surface of the Ni foam has a relatively uniform coverage of Pt particle. This further suggests that small Pt particles, most of which are too small to observe in the SEM images, contribute significantly to the observed Pt EDS signal and to the subsequently studied properties of the Pt modified Ni foams.

Electrochemical Behavior of Pt/Ni Foams in Alkaline Media. Cyclic voltammetry (CV) was used to examine the electrochemical properties of Pt/Ni foams in aqueous alkaline electrolyte and to compare the electrochemical behavior of Pt/Ni foams to that of unmodified Ni foam and bulk Pt(poly). Figure 3 shows overlaid CV profiles in the $0.05 \leq E \leq 1.30$ V

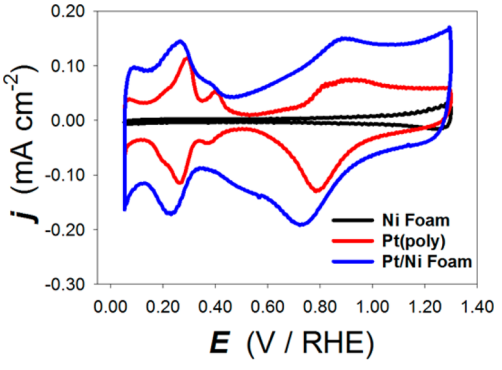

Figure 3. Overlaid cyclic voltammetry profiles collected for Ni foam (black), Pt/Ni foam (blue), and Pt(poly) (red); each was collected in 0.50 M KOH at T = 293 K with s = 100 mV s^{-1}.

range for unmodified Ni foam (black curve), Pt/Ni foam (sample type BB 10; blue curve), and Pt(poly) (red curve), each acquired in 0.50 M aqueous KOH electrolyte at T = 298 K

and at a scan rate (s) of 100 mV s^{-1}. A typical CV profile for Pt(poly) in aqueous KOH or NaOH solution in this E range displays the following features: (i) the under-potential deposition of hydrogen (H_{UPD}) adsorption (cathodic) and desorption of H_{UPD} (anodic) at $0.05 \leq E \leq 0.45$ V; (ii) the capacitive double-layer region, $0.45 \leq E \leq 0.80$ V; (iii) the formation of PtO at $E \geq 0.80$ V (anodic); and (iv) the reduction of PtO (cathodic) at $0.50 \leq E \leq 1.20$ V.[13]

The CV profile of unmodified Ni foam is essentially featureless in this potential range. From 0.05 V to ca. 0.70 V a small, steady double-layer current density (j) is observed; there is a very gradual increase in j at $E > 0.70$ V that corresponds to the formation of β-$Ni(OH)_2$.[44] The CV profile of Pt/Ni foam is plotted in blue and displays similar features to that of Pt(poly) (the red curve). Here, we observe the expected cathodic and anodic H_{UPD} features at $0.05 \leq E \leq 0.45$ V. The anodic j corresponding to the formation of PtO dominates the upper potential region, and the cathodic j corresponding to the reduction of PtO is observed at $E \leq 1.20$ V. However, in the case of Pt/Ni foam, the H_{UPD} peaks are broad indicating that the deposited Pt does not have well-defined crystal facets.[49,50] It is difficult to discern a well-defined double layer region in the CV profile of Pt/Ni foam. In the cathodic half of the CV profile, the reduction of PtO is spread out over a large E range that overlaps the expected double-layer region and the onset of H_{UPD} adsorption. In the anodic half of the CV profile, there is a minimum in j that consistently occurs in the $0.40 \leq E \leq 0.50$ V range. The position of this minimum is related to the completion of the H_{UPD} desorption and anion adsorption. The increase in j beyond $E = 0.50$ V is due to the onset of PtO formation, which occurs at potentials lower than those observed for Pt(poly).

Electrochemically Active Surface Area and Mass Loading of Pt on Pt/Ni Foams. The electrochemically active surface area (A_{ecsa}) of deposited Pt was determined for at least three separate Pt/Ni foam disks of each sample type. The Pt/Ni disks were mounted as working electrodes and then subjected to a minimum of 200 CV cycles in 0.5 M aqueous KOH at $s = 100$ mV s^{-1}. The shape of the CV profile for Pt/Ni foams evolves significantly during these 200 CV cycles; this behavior is analyzed in detail in an upcoming section. The 200th CV cycle was chosen for the A_{ecsa} determination because, at this point, the most significant changes in the CV profiles had already occurred. Using the 200th CV profile, the charge corresponding to H_{UPD} desorption is determined by first isolating the anodic section from $E = 0.05$ to 0.45 V and then subtracting from this section the value of I at $E = 0.45$ V. This I value corresponds to the minimum I observed in the double-layer region; it is accepted as an estimate of the double-layer current (I_{DL}). By subtracting I_{DL}, the remaining I is attributed to the pseudocapacitive current associated with the desorption of H_{UPD}. This section of the CV profile is integrated to obtain the charge (Q), which is converted to A_{ecsa} using the value of 220 μC cm^{-2} that is the charge density of H_{UPD} monolayer adsorption on Pt(poly).[51,52] Since the CV profile for the unmodified Ni foam displays no features in the E region corresponding to H_{UPD} adsorption and desorption, in the case of Pt/Ni foams all of the I features in this region are attributed to the combination of the H_{UPD} desorption process at the deposited Pt and the double-layer charging. The H_{UPD} desorption method is the most popular and most reliable approach for determining A_{ecsa} of Pt(poly) electrodes; it is considered reliable for Pt nanoparticles and large surface area Pt materials.[52]

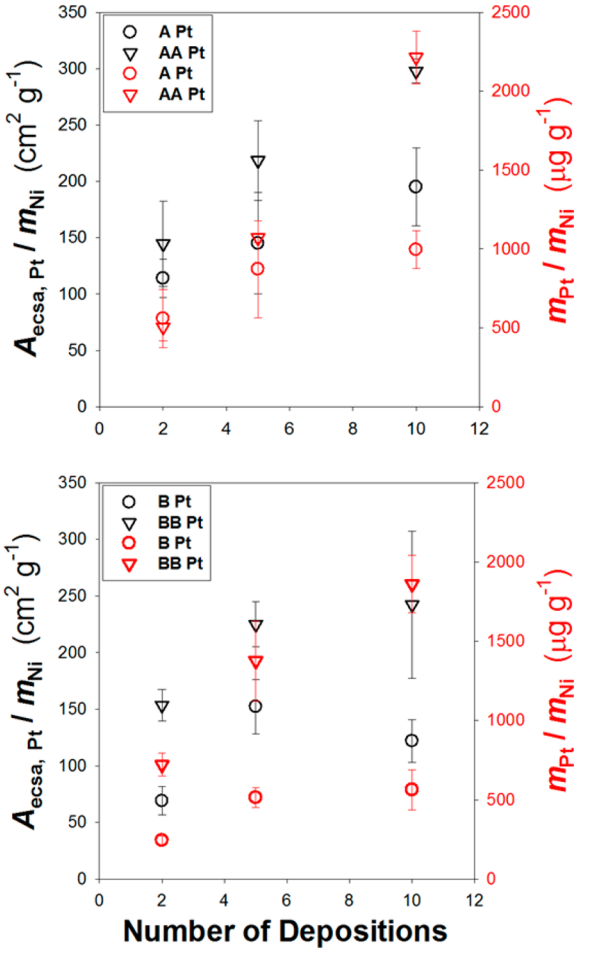

Figure 4. Relationship between the number of deposition events, the electrochemical surface area of platinum ($A_{ecsa,Pt}$, black symbols), and the mass of deposited Pt per mass of Ni foam (m_{Pt}/m_{Ni}, red symbols), as measured by ICP-OES. The top graph shows the data for Pt deposited from a K_2PtCl_4 salt solution (A and AA samples); the bottom graph shows the data for Pt deposited from a K_2PtCl_6 salt solution (B and BB samples).

The mass loading of Pt on each type of Pt/Ni foam was determined using ICP-OES. Figure 4 presents two graphs that show A_{ecsa} of deposited Pt per unit of mass of Ni foam ($A_{ecsa,Pt}/m_{Ni}$ in cm^2 g^{-1}) and the mass loading of Pt per unit of mass of Ni foam (m_{Pt}/m_{Ni} in μg g^{-1}) for each sample type. The top graph displays the $A_{ecsa,Pt}/m_{Ni}$ and m_{Pt}/m_{Ni} values for the type A and AA samples; the bottom graph displays the $A_{ecsa,Pt}/m_{Ni}$ and m_{Pt}/m_{Ni} values for the type B and BB samples. Each point in these two graphs represents a value obtained from averaging three separate specimens; the error bars reflect the standard deviation.

A careful analysis of the data presented in Figure 4 allows some general trends to be observed. For both the type A and type AA samples, there is a linear increase in A_{ecsa}/m_{Ni} as the number of depositions increases from 2 to 5 to 10. The slope of the line representing the relationship between $A_{ecsa,Pt}/m_{Ni}$ and the number of depositions is the steepest for the type AA samples, likely due to the higher concentration of Pt in the deposition solution used to make the AA samples. However, doubling the concentration of Pt in the deposition solution does not result in a 2-fold increase in the value of $A_{ecsa,Pt}/m_{Ni}$;

rather, the ratio between the $A_{ecsa,Pt}$ of the AA samples (prepared from a Pt solution with 2 times the concentration of Pt compared to A samples) and $A_{ecsa,Pt}$ of the A samples is slightly less than 1.5. The ratio between the $A_{ecsa,Pt}/m_{Ni}$ values for the AA samples and the A_{ecsaPt}/m_{Ni} values for the A samples is slightly less than 1.5. The relationship between m_{Pt}/m_{Ni} and the number of depositions is not linear for the type A samples; in this case the mass of deposited Pt seems to level off after five depositions. With respect to the AA samples, the relationship between m_{Pt}/m_{Ni} and the number of depositions is linear. After 10 deposition events, the mass of Pt on the type AA samples is more than double the mass of Pt on the type A samples. However, this large difference in m_{Pt}/m_{Ni} values is not observed between the type A and AA samples with two and five depositions; on the contrary, at two and five depositions, the Pt mass loading of the type A and AA samples overlap within experimental uncertainty. Similar trends are observed in the bottom graph of Figure 4, which displays the data obtained for the B and BB type samples. For both the type B and BB samples, the $A_{ecsa,Pt}/m_{Ni}$ increases from two to five depositions, but levels off or decreases slightly for those samples with 10 deposition events. A comparison of the B and BB type samples demonstrates an approximately 2-fold increase in $A_{ecsa,Pt}/m_{Ni}$ by doubling the concentration in the deposition solution. The relationship between m_{Pt}/m_{Ni} and the number of depositions is not linear for the B or BB type samples. The average value of m_{Pt}/m_{Ni} levels off after five deposition events for the type B samples and increases for the BB type samples. Doubling of the concentration of Pt in the K_2PtCl_6 deposition solution results in a 2.5−3.5 fold increase in the value of m_{Pt}/m_{Ni}. Overall, the trends observed in both graphs of Figure 4 indicate that the $A_{ecsa,Pt}/m_{Ni}$ and m_{Pt}/m_{Ni} values achieved for various numbers of depositions are similar for the two Pt compounds employed. The B- and BB-type samples, on average, have slightly lower A_{ecsa}/m_{Ni} and m_{Pt}/m_{Ni} values as compared to the A- and AA-type samples.

The trends observed indicate significant differences between the deposition properties of the Pt^{4+} and Pt^{2+} salt solutions, and their concentrations in solution, that have important implications on the final properties of the Pt/Ni foams. Because of the high cost of Pt, it is optimal for the final Pt/Ni foams to have a large ratio of $A_{ecsa,Pt}/m_{Pt}$ (Pt mass enhancement factor), as to maximize the use of Pt for electrocatalytic application. Therefore, in Figure 4, it is desirable for the difference between Pt mass loading expressed as m_{Pt}/m_{Ni} (the red points) and the Pt surface area expressed as $A_{ecsa,Pt}/m_{Ni}$ (the black points) to be large, such that a small Pt mass loading translates into a large $A_{ecsa,Pt}$. A large value of the $A_{ecsa,Pt}/m_{Pt}$ ratio indicates that the Pt deposits on these samples are generally small in size, as to optimize the surface area-to-volume ratio of Pt particle coatings. The AA samples exhibit a high Pt mass enhancement factor (relative to the other Pt/Ni foams) after the first deposition event and after five deposition events, but this good mass enhancement is not observed after 10 deposition events. This trend is not consistent for the A samples, indicating that the seeding of Pt particles is highly sensitive to the Pt salt concentration. For the AA samples, the trend suggests that the Pt salt seeds uniformly cover the Ni surface to produce small Pt particles well-dispersed over the Ni foam surface. The Pt particles then continue to grow with repeated deposition cycles. After 10 deposition events, the Pt particles become large and agglomerate, resulting in the decreased mass enhancement. Similar to the A and AA samples, the trends observed for the B and BB samples are not consistent, further emphasizing the impact of concentration on the morphology of Pt deposits. The largest mass enhancement for these samples is shown for the sample type B after five deposition cycles. In general, the correlation between m_{Pt} and $A_{ecsa,Pt}$ observed for the Pt^{4+} salt solutions suggests the Pt deposits tend to form larger particles from the outset, resulting in a small mass enhancement. The lower concentration of sample type B (compared to BB) likely allows for multiple deposition cycles to produce smaller Pt deposits that more uniformly cover the surface, resulting in the maximum observed after five deposition events. This difference in seeding process for the A and AA as well as the B and BB samples can be explained through differences in the energy required to reduce Pt^{2+} and Pt^{4+} salts. The Pt^{2+} salts should be more readily reduced in the $NaBH_4$ solution used for electroless deposition, making it more energetically favorable for multiple seeds to be produced throughout the Ni foam and resulting in small, well-dispersed Pt deposits. The Pt^{4+} salts require more energy for reduction onto the Ni surface, such that the conditions will favor the formation of fewer seeds and result in larger Pt deposits.

Stability of the Pt/Ni Foams as Revealed by Potential Cycling. Potential cycling was employed to examine in detail how the CV profile of Pt/Ni foam changes over the course of several hundred of transients that can be related to the material's stability in an electrochemical environment. Figure 3 shows CV profiles for the unmodified Ni foam, Pt(poly), and Pt/Ni foams; the j values in the double-layer region of these materials are 2.41, 10.78, and 41.45 μA cm^{-2}, respectively. These j values can be converted to double-layer capacitance (C_{DL}) by dividing them by s; such calculated C_{DL} values for the unmodified Ni foam, Pt(poly), and Pt/Ni foam are 0.241, 1.08, and 4.15 F m^{-2}, respectively. The C_{DL} value of an electrode is affected by several factors including the roughness and geometry of the electrode, the electrode surface area, the nature of the electrolyte, and electronic properties of the electrode material that impact its interaction with the electrolyte.[52,53] When comparing the Pt/Ni foams to either the unmodified Ni foam or Pt(poly), it is necessary to remember that by depositing Pt on the Ni foam, we altered the roughness and surface area of the electrode and added a new material to the system. Thus, it is not unreasonable to observe a large change in the C_{DL} of the modified material.

Changes that occur in the CV profile for Pt/Ni foam during repetitive potential cycling are examined in the three graphs of Figure 5. Graph A displays the first 400 CV profiles in the $0.05 \leq E \leq 1.30$ V range collected in 0.50 M aqueous KOH at $T = 293$ K and $s = 100$ mV s^{-1}. The profiles are color-coded in groups of 50 cycles. It is evident from Figure 5A that the majority of changes in the CV profiles occur in the first 100 CV transients. During the 400 CV scans, the CV profile of Pt/Ni foam evolves from its original appearance to resemble more closely the shape expected for Pt(poly) in aqueous alkaline media. The following changes are observed in the CV profile of Pt/Ni foam during the 400 CV scans.

(i) Significant changes occur in the forward scan of the CV profile in the $0.60 \leq E \leq 0.90$ V range. A peak centered at ca. 0.80 V in the first few cycles decreases in intensity and eventually disappears with potential cycling, as indicated by the black arrow.

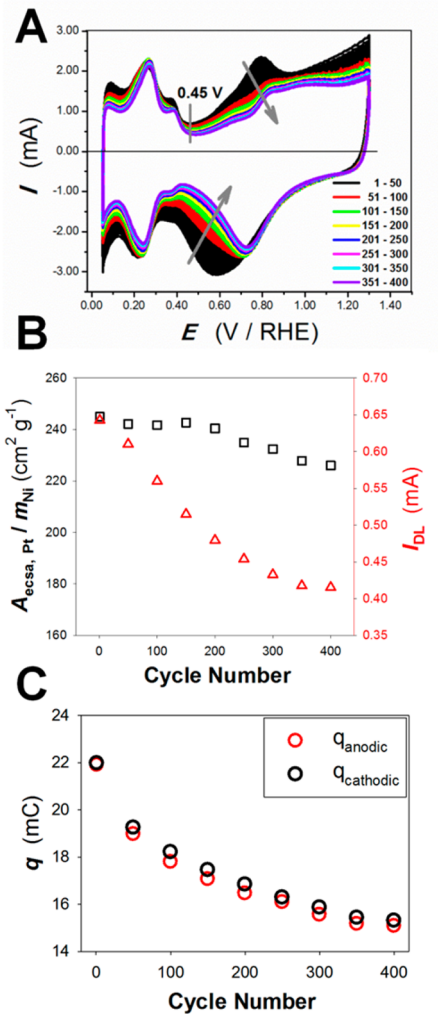

Figure 5. (A) 400 cyclic voltammetry profiles for Pt/Ni foam collected in 0.50 M KOH at T = 293 K with s = 100 mV s^{-1}. The CV profiles are in groups of 50 cycles, according to color. (B) Relationship between the cycle number, the electrochemical surface areas of Pt ($A_{ecsa,Pt}$, black squares), and double-layer current (I_{DL}) from the CV profile (red triangles). (C) The total anodic and cathodic charges (Q_{anodic}, $Q_{cathodic}$) from 0.05 ≤ E ≤ 1.30 V as a function of cycle number.

(ii) There is a decrease in I throughout the entire PtO formation region. After approximately the first 200 cycles, the loss of I appears to be uniform in the 0.70 to 1.30 V potential range.

(iii) In the reverse scan, within the potential range of 0.70 ≤ E ≤ 0.30 V, I decreases significantly with potential cycling. This decrease is most significant in the first 100 cycles. This E region also gives the appearance of the PtO reduction peak shifting toward slightly higher potential values (indicated by the black arrow). The shape of the PtO reduction peak does not change on the upper-potential side of the peak maximum (E > 0.75 V).

(iv) Major changes are observed in the double-layer region of the CV profile (near E = 0.45 V). This is of particular importance because the A_{ecsa} values of Pt on the Pt/Ni foams are calculated using the charge of H_{UPD} desorption in the CV profile, which requires knowledge of the double-layer current (I_{DL}). The I_{DL} value, as measured at E = 0.45 V, decreases significantly during the first 200 CV cycles. After 200 potential cycles the decrease in I_{DL} as a function of CV scan number begins to level off. In the forward scan, the thick double-layer region overlaps with the onset of PtO formation that occurs between E = 0.60 and 0.80 V. On the basis of these repetitive CV measurements, it is hard to define at which potential PtO formation begins.

(v) There is some decrease in I in the H_{UPD} region (both anodic and cathodic). In the first 200 CV scans, the peaks corresponding to H_{UPD} adsorption and desorption become shaper and more well-defined; this is indicative of restructuring of the deposited Pt and possible grain growth because the peaks in this region correspond to particular crystal facets of a polycrystalline material.[49,50,54] After the first 200 cycles, the decrease in I in this region is uniform over the H_{UPD} adsorption potential range, and the shape of peaks remains the same. This is indicative of overall loss of A_{ecsa} of Pt most likely via detachment of Pt particles and electrodissolution of Pt.[55,56]

Figure 5B shows calculated $A_{ecsa,Pt}/m_{Ni}$ values for one Pt/Ni foam electrode as well as the measured value of I_{DL} (I at E = 0.45 V) plotted as a function of CV scan number for a BB 10-type sample. This analysis was carried out for five different Pt/Ni foam samples; the results presented are representative of all five samples. Graph B shows a decrease in the value of $A_{ecsa,Pt}/m_{Ni}$ over the 400 CV transients. After the 400 CV scans, the value of $A_{ecsa,Pt}/m_{Ni}$ decreased by about 19 cm^2 g^{-1}, which corresponds to ca. 8% of the initial $A_{ecsa,Pt}/m_{Ni}$ value. Within the five samples that were examined in this manner, the average loss of $A_{ecsa,Pt}/m_{Ni}$ was 13% over the course of 400 cycles. The decrease in $A_{ecsa,Pt}/m_{Ni}$ may have a number of different origins: (i) detachment of Pt particles; (ii) decrease in surface area through rearrangement, grain growth, and smoothing of the surface;[54] and (iii) electrochemical dissolution of Pt as a result of potential cycling.[56,57] Figure 5B also shows a decrease in I_{DL} as a function of CV transient number. Here, we observe a sharp, linear decrease over the initial 200 cycles, and the value of I_{DL} begins to level off for the cycle number 350 and 400.

Figure 5C shows the total anodic charge (Q_{anodic}) and total cathodic charge ($Q_{cathodic}$) from the CV profile of Pt/Ni foam (0.005 ≤ E ≤ 1.30 V), plotted as a function of the CV transient number. This plot demonstrates that the values of Q_{anodic} and $Q_{cathodic}$ are very similar to each other throughout the 400 CV scans; however, in all cases $Q_{cathodic}$ is slightly higher than Q_{anodic}. In the CV profile for Pt/Ni foams, the onset of HER is visible at E < 0.10 V in the cathodic CV scans. The small difference between $Q_{cathodic}$ and Q_{anodic} is attributed to onset of HER, which contributes only to the cathodic current of the CV profile. Both Q_{anodic} and $Q_{cathodic}$ decrease drastically over the initial 200 potential cycles and then begin to level off. Since Q_{anodic} and $Q_{cathodic}$ are approximately equal, we cannot attribute the drastic changes in the CV profile over the 400 CV scans to the oxidation of impurities because, in such a case, we would expect Q_{anodic} to be significantly larger than $Q_{cathodic}$ for a given cycle number. On the basis of the evidence presented in the three graphs of Figure 5, we conclude that the changes observed in the CV profile of Pt/Ni foam as potential cycling progresses are the result of several concurrently occurring processes that include the restructuring of deposited Pt and loss of Pt through the detachment of Pt particles and electrodissolution of Pt. We wish to add that we did attempt to further confirm the restructuring and crystal grain growth of the

deposited Pt using X-ray diffraction (XRD). The goal was to examine the average grain size of Pt as a function of CV scan number using XRD data and the Scherrer formula.[54,58] Unfortunately, because of the low loading of Pt and the open porous morphology of the Pt/Ni foams, the intensity of the Pt XRD peaks was too low for quantification.

Part 2: Electrocatalytic Activity of Pt/Ni Foams. In this section, we examine the electrocatalytic activity of Pt/Ni foams toward HER, HOR, ORR, and OER. The reactions were carried out via the LSV and Tafel polarization methods using Pt/Ni foams of each type (A, AA, B, and BB with 2, 5, and 10 deposition events). Unmodified Ni foam and Pt_{poly} electrodes were also included in the analysis for comparison. The characterization results presented above demonstrate that the Pt particles deposited from solutions containing either K_2PtCl_4 or K_2PtCl_6 are very similar in terms of particle size and morphology, and the CV profiles obtained for the various Pt/Ni foams display identical behavior. With this in mind, we proceed to interpret the following electrocatalysis results by considering the four different electrode types (A, AA, B, and BB) with various numbers of deposition events (2, 5, and 10) as one large sample set. The variable that we consider within this sample set is the A_{ecsa} of Pt, which we determine for each individual Pt/Ni foam electrode. In the upcoming analysis, we quantify the amount of Pt on a Pt/Ni foam electrode in terms of the A_{ecsa} of Pt divided by the total A_{ecsa} of the electrode (A_{ecsa} Pt + A_{ecsa} Ni foam). The Pt/Ni foams are bimetallic materials that present a unique challenge in defining and determining the electrochemically active surface area that should be used when converting the I values to j values to compare the various electrodes. Generally, the I measured in an electrochemical experiment is converted to current density by normalizing the I to the A_{ecsa} of the electrode. This allows comparisons to be made between electrodes that have different A_{ecsa} values. In previous studies, we presented methods used to estimate the A_{ecsa} of the Ni foam substrate and relate the Ni A_{ecsa} to the mass of the Ni foam electrode.[44,45] The specific surface area ($A_s = A_{ecsa}/m$) of the Ni foam used in this study was, therefore, estimated from these previous studies and is ca. 300 $cm^2\ g^{-1} \pm 90\ cm^2\ g^{-1}$.[45] The total A_{ecsa} of a Pt/Ni foam electrode is determined by adding the A_{ecsa} of Pt, determined via CV analysis of the adsorption of H_{UPD}, to the A_{ecsa} of the Ni foam support. For any given Pt/Ni foam electrode, the experimental uncertainty associated with the total A_{ecsa} value is dominated by the large uncertainty (30%) associated with the A_s of Ni foam. There is also some uncertainty associated with the determination of Pt A_{ecsa} using the H_{UPD} method described above because the CV profile of Pt/Ni foams never completely stabilize as a result of structural changes in the Pt deposit (particle detachment, agglomeration, and dissolution). To evaluate the significance of this uncertainty on the analysis of Pt/Ni foam electrocatalytic performance, the A_{ecsa} of Pt for eight separate Pt/Ni electrodes was determined before and after HER and HOR experiments. These values differed by an average of 4%, indicating that the A_{ecsa} calculated after the HER and HOR measurements is also representative of the electrode before these measurements. The determination of j for the HER, HOR, ORR, and OER with Pt/Ni foam electrodes is further complicated by the fact that both Pt and Ni are electrocatalytically active for some of the reactions studied and that their activities differ significantly. In some cases, it is not obvious if the A_{ecsa} of the Ni foam substrate should be included in the calculation of j values. This issue is addressed independently for each of the reactions studied.

The Hydrogen Evolution Reaction. Both Ni and Pt are considered good electrocatalysts for the HER in alkaline media. The exchange current density of the HER ($j_{o,HER}$) for a Pt cathode is about 2.5 orders of magnitude higher than that of a Ni cathode.[59] Figure 6A shows LSV profiles for the HER occurring at the unmodified Ni foam, Pt(poly), and three Pt/Ni foams with various $A_{ecsa,Pt}$ values, as indicated by the ratio $A_{ecsa,Pt}/A_{ecsa,total}$, where the total electrochemically active surface area ($A_{ecsa,total}$) is the sum of the electrochemically active surface area of Pt ($A_{ecsa,Pt}$) and the electrochemically active surface area of Ni ($A_{ecsa,Ni}$); thus, $A_{ecsa,total} = A_{ecsa,Pt} + A_{ecsa,Ni}$. Because the scan rate was very low, the current density reached at every E value corresponded to a near steady-state current density. The E values for all electrocatalysis measurements presented herein are corrected for IR drop. The current density for the HER (j_{HER}) at the Ni foam (purple LSV profile) is very low as compared to that of Pt(poly) (blue LSV profile) and that of the Pt/Ni foams (black, red, and green LSV profiles, respectively). Although the Ni foam is significantly less active toward HER than the Pt/Ni foams, there is a small j observed as E approaches −0.15 V. All of the materials that contain Pt (i.e., Pt(poly) and the Pt/Ni foams) display significant j, even at small overpotential values. The Ni foam electrode does not produce any measurable j for the HER in the initial 20 mV of the LSV scan. Since both Ni and Pt are active electrocatalysts toward the HER, the LSV profiles for Pt/Ni foams are normalized by dividing the experimental I value by $A_{ecsa,total}$ to obtain the value of j. The LSV profiles for the Pt/Ni foams demonstrate increasing j_{HER} with increase in $A_{ecsa,Pt}$. The Pt/Ni foam with the highest $A_{ecsa,Pt}$ (green LSV profile, $A_{ecsa,Pt}$ equals ca. 46% of $A_{ecsa,total}$) demonstrates electrochemical behavior that is very similar to that of Pt(poly) in this potential range.

Figure 6B shows the j_{HER} values obtained at $E = -0.150$ V for the Pt/Ni foam electrodes, as well as for the unmodified Ni foam and Pt(poly). These values were obtained from the LSV profiles and are plotted as a function of $A_{ecsa,Pt}/A_{ecsa,total}$. The j_{HER} values for the unmodified Ni foam and Pt(poly) are shown as green and blue circles, respectively. To facilitate a comparative data analysis, we add dotted horizontal lines that represent the j_{HER} values for the untreated Ni foam and Pt(poly). The black circles represent the j_{HER} values obtained when I is divided by $A_{ecsa,total}$. In this case, both the deposited Pt and the underlying Ni foam act as electrocatalytic materials at which HER takes place. The red triangles represent the j_{HER} values obtained when I is divided by only $A_{ecsa,Pt}$. In this case, the Ni foam is considered electrocatalytically inactive, and the entire I for HER is attributed to the deposited Pt particles. In all cases, the j_{HER} values obtained when I is normalized to only the $A_{ecsa,Pt}$ (the red triangles) is greater than the j_{HER} of Pt(poly).

A number of different explanations can account for this apparent improvement in the catalytic activity of Pt contained in Pt/Ni foams, in comparison to Pt(poly) toward HER. These include (i) enhanced activity of Pt toward HER due to electronic interactions between Pt and Ni, (ii) activity of the underlying Ni foam support toward HER, and (iii) improved diffusion of reactants and products to and from the Pt surface resulting in more efficient catalytic turnover. There are a number of studies that report increased electrocatalytic activity through the addition of Ni to Pt electrode materials.[60−63] These increases in electrocatalytic activity are often attributed to a change in the Pt−Pt bond distance or electronic effects brought

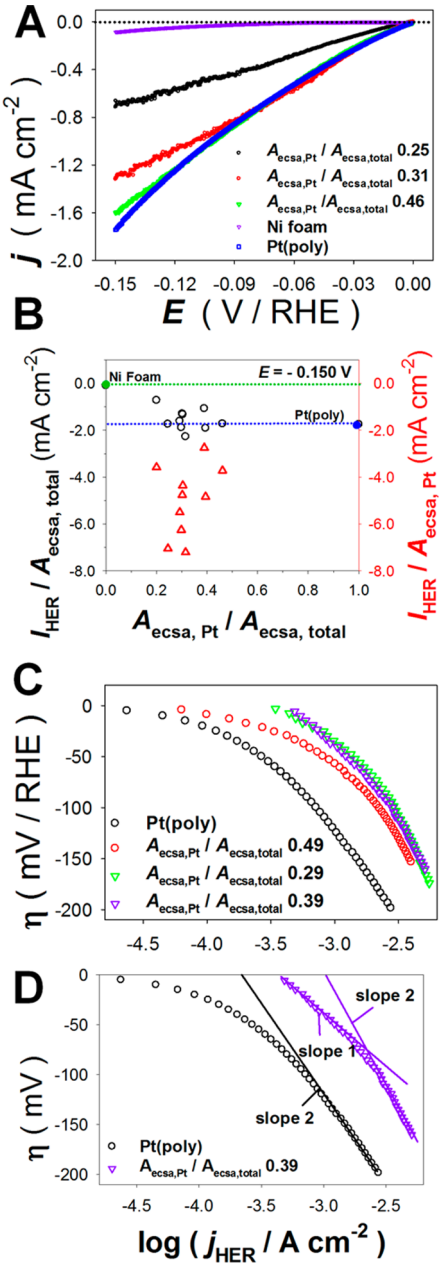

Figure 6. (A) Linear sweep voltammetry (LSV) profiles for the hydrogen evolution reaction (HER) in 0.50 M KOH using the following electrodes: Ni foam (purple); Pt(poly) (blue); and Pt/Ni foams with different $A_{ecsa,Pt}/A_{ecsa,total}$ ratios: 0.25 (black), 0.31 (red), 0.46 (green); s = 0.1 mV s^{-1}, T = 293 K. (B) HER current density (j_{HER}) values at E = −0.150 V for Pt(poly), Ni foam, and Pt/Ni foam electrodes with various $A_{ecsa,Pt}/A_{ecsa,total}$ ratio values; these values are obtained from LSV profiles. Black circles correspond to j_{HER} values normalized to $A_{ecsa,total}$; red triangles correspond to j_{HER} values normalized to $A_{ecsa,Pt}$. (C) HER Tafel polarization plots for Pt(poly) (black), and Pt/Ni foam electrodes with various $A_{ecsa,Pt}/A_{ecsa,total}$ ratios: 0.49 (red), 0.29 (green), 0.39 (purple) carried out in 0.50 M KOH at T = 293 K. (D) Illustration for the determination of the Tafel slope (b) and exchange current density ($j_{o,\,HER}$) from Tafel polarization curves of Pt(poly) and Pt/Ni foam electrodes.

about by the added metal, such as an increase in its d-vacancy character.[60] Binary NiPt electrocatalysts were developed and examined for their suitability for reactions such as HOR and ORR, CO oxidation, methanol oxidation.[60−63] During the preparation of the Pt/Ni foams, we did not include any specific steps as to alloy the deposited Pt to the Ni foam, and so these electronic effects are anticipated to be minimal. The LSV plot in Figure 6 demonstrates that the unmodified Ni foam has low activity toward the HER. A previous study of the HER using a polycrystalline Ni electrode showed that a freshly polished metallic Ni electrode is more active toward HER than the same electrode after the electrochemical formation of surface oxides.[64] In that study, it was observed that j_{HER} decreased by an order of magnitude after the polished electrode was oxidized.[64] It is possible that our $NaBH_4$ treatment of the Ni foams during Pt deposition could have improved the activity of Ni toward HER through the reduction, or partial reduction, of the native surface oxide (β-Ni(OH)$_2$) on the surface of Ni foam. This likely does not account for all j gains shown for the Pt/Ni foams as compared to Pt(poly). Most likely, the greatest improvements in the Pt activity are a result of improvements in diffusion. Mass transport to and from the surface of small spherical Pt particles, such as those present in the Pt/Ni foams, is three-dimensional, rather than linear, resulting in an increased current density. This effect is further illustrated in our examination of the Pt/Ni foam and Pt(poly) Tafel plots.

Figure 6C presents Tafel polarization plots for HER taking place on Pt(poly) and on three Pt/Ni foams with different values of $A_{ecsa,Pt}$. From this graph, it is evident that Pt(poly) and the Pt/Ni foams reveal different electrochemical behaviors. Figure 6D shows the Tafel plot for Pt(poly) and one Pt/Ni foam in more detail. The plot corresponding to Pt(poly) has a linear region for the overpotential from η = −100 to η= −200 mV range. The Tafel plot corresponding to the Pt/Ni foam has two linear regions, one at lower absolute η values (−100 < η < 0 mV) and one at higher absolute η values (η < −120 mV). In general, the information obtained from Tafel plots can be used to determine mechanistic information about an electrochemical process and also to compare the electrocatalytic activity of various electrocatalysts. The Tafel slope (b) is the slope of the linear portion of a η versus log j curve. The Tafel slope depends not only on the reaction mechanism and the material's intrinsic activity toward the process, but also on its three-dimensional structure, porosity, and presence of grains that possess their unique surface arrangement of atoms and electrocatalytic activities. Identification of a linear region and its extrapolation to η = 0 mV allows the determination of the exchange current density (j_o) of the electrode process. The presence of more than one linear region might be attributed to a given reaction possessing two different mechanistic pathways, provided that other phenomena do not give rise to a different Tafel slope. At high overpotential values, Tafel polarization curves reveal a nonlinear relationship, and j values gradually reach a limiting value because the process is under mass-transport control. In the case of multicomponent electrodes, Tafel polarization plots are difficult to analyze because the same reaction can occur at different rates at different components and can also have different reaction mechanisms. In the case of Pt/Ni foams, the Tafel plots are not analyzed for mechanistic information because HER occurs simultaneously on Pt and Ni. However, the Tafel plots for HER for Pt/Ni foams shown in Figure 6C may be used to determine j_o and b to perform a comparative analysis of their activities and to relate them to the respective j_o and b values for Pt(poly). Table 1 presents the j_o and b values obtained from the HER Tafel plots. The Tafel plot for Pt(poly) has only one linear region. Because it is observed at high η values and because it is in the same overpotential range as the

Table 1. Exchange Current Density and Tafel Slope Values for HER and OER Using Ni Foam, Pt_{poly}, and Pt/Ni Foam Electrodes

electrode material	j_o (1) A cm^{-2}	b (1) mV/dec	j_o (2) A cm^{-2}	b (2) mV/dec
HER				
Ni foam	1.0×10^{-5}	-120 ± 10	4.9×10^{-6}	-180 ± 15
Pt(poly)			1.8×10^{-3}	-170 ± 15
Pt/Ni foam	3.9×10^{-4}	-90 ± 5	1.0×10^{-3}	-230 ± 20
OER				
Ni foam	1.0×10^{-11}	40 ± 5	1.4×10^{-4}	320 ± 30
Pt(poly)	2.8×10^{-11}	60 ± 5	5.3×10^{-5}	330 ± 30
Pt/Ni foam	3.8×10^{-10}	60 ± 5	8.6×10^{-5}	350 ± 30

second linear region of the Pt/Ni foams, it is arbitrarily defined as a linear region 2. The b value for Pt(poly) is the lowest, which is expected due to the superior electrocatalytic activity of Pt toward this reaction. Our $j_{o,HER}$ = 1.8 mA cm^{-2} and b = -170 ± 15 mV/dec slightly differ from the literature values of $j_{o,HER}$ = 1.03 mA cm^{-2} and b = 130 mV/dec in alkaline solution at T = 293 K.[22] The difference in $j_{o,HER}$ is small and within the experimental uncertainty, while the difference in b could be assigned to the nonplanar electrode geometry (a wire-shaped Pt(poly) electrode).

The Hydrogen Oxidation Reaction. Figure 7A shows LSV profiles for HOR taking place on the unmodified Ni foam, Pt(poly), and three Pt/Ni foams with various $A_{ecsa,Pt}$ values. The LSV profiles were collected in the $0.000 \le E \le 0.200$ V region, in 0.50 M aqueous KOH electrolyte saturated with H_2 (g, 1 atm), at T = 293 K, and with s = 0.1 mV s^{-1}; the electrolyte was stirred during the measurement. The main graph in Figure 7A shows the HOR LSV profiles using the same j-axis scale (y-axis) as in the HER LSV profiles shown in Figure 6A. This demonstrates that j_{HOR} is significantly lower than j_{HER} for both Pt(poly) and the unmodified Ni foam. The inset in Figure 7A shows the same HOR LSV profiles but using an enlarged scale. These LSV profiles demonstrate that the unmodified Ni foam has essentially no electrocatalytic activity toward HOR; the j_{HOR} for Ni foams is on the order of 10^{-7}A cm^{-2}. In general, polycrystalline Ni is not considered a good electrocatalyst for the HOR; however, some activity is expected. According to an extensive analysis of the HOR using polished polycrystalline Ni electrodes, the expected j_{HOR} in alkaline solution using a freshly polished Ni electrode is approximately 20 μA cm^{-2}. In the same study,[12] the authors observe that the HOR begins in the reverse scan of a CV experiment only once the α-$Ni(OH)_2$ surface oxide has been reduced, suggesting that HOR does not proceed when the electrode surface is covered with an oxide. The surface of the unmodified Ni foam used in this study is covered with β-$Ni(OH)_2$, which forms spontaneously when Ni is in contact with the ambient; this oxide cannot be reduced electrochemically.[45] The presence of this surface oxide on Ni foam is likely responsible for its inactivity toward the HOR reported in this study. The LSV profile for Pt(poly) shows that it is an active electrocatalyst for HOR. The LSV profiles for the Pt/Ni foams display a very unexpected, though reproducible, behavior. The Pt/Ni foams display moderate activity toward HOR, as compared to Pt(poly). However, an overpotential in the $50 \le \eta \le 100$ mV range is required to observe any significant anodic j. The most unexpected behavior of the Pt/Ni foams (but not of the unmodified Ni foam) is a cathodic current density in the $0 \le \eta \le 100$ mV range. In addition, the same behavior is observed in

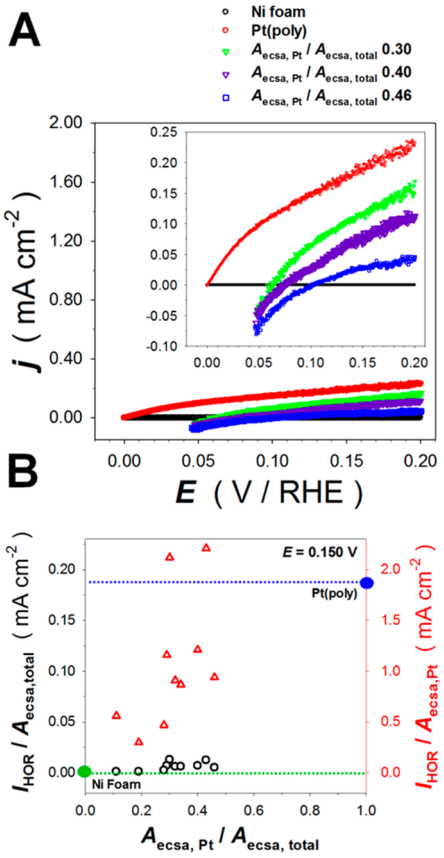

Figure 7. (A) Linear sweep voltammetry (LSV) profiles for the hydrogen oxidation reaction (HOR) in 0.50 M KOH using the following electrodes: Ni foam (black); Pt(poly) (red); and Pt/Ni foams with different $A_{ecsa,Pt}/A_{ecsa,total}$ ratio values: 0.30 (green), 0.40 (purple), 0.46 (blue); s = 0.1 mV s^{-1}, T = 293 K. (B) HOR current density (j_{HOR}) values at E = 0.150 V for Pt(poly), Ni foam, and Pt/Ni foam electrodes with various $A_{ecsa,Pt}/A_{ecsa,total}$ ratio; these values are obtained from LSV profiles. Black circles correspond to j_{HER} values normalized to $A_{ecsa,total}$; red triangles correspond to j_{HER} values normalized to $A_{ecsa,Pt}$.

HOR Tafel polarization measurements (not shown) that are carried out immediately following the completion of the HOR LSV measurements. As described in the Experimental Section, the HOR measurements were performed immediately after the examination of HER, and the Pt/Ni foams were not exposed to any potential cycling; the measurements were carried out in the same electrolyte without the electrode being removed from the electrochemical cell. Thus, the Pt/Ni foams were not covered with any oxide species that could be reduced electrochemically

(such as Pt surface oxide or α-Ni(OH)$_2$ on Ni) and could give rise to a cathodic current during the examination of HOR kinetics. It is also very unlikely that the electrolyte contained impurities that could result in a cathodic current. In fact, any impurities present in the electrolyte would affect the shape of CV profiles of Pt(poly) or Ni. Therefore, the above-reported cathodic current density observed in the $0 \leq \eta \leq 100$ mV range may not be attributed to the reduction of surface oxide or reduction of impurities. At this stage, we are unable to explain the exact origin of this cathodic current and provide experimental evidence for the correctness of our explanation but report this behavior because it is reproducible. The only explanation, which is very speculative and without any evidence, is that the negative current density is due to cathodic H absorption into the Ni foam that mediated by Pt nanoparticles. However, we would also like to note that this is not the first study to report a cathodic current density at positive η values for supported Pt electrocatalysts. A similar behavior was observed for Pt particles dispersed in a polyaniline matrix on a glassy carbon support during LSV measurements in the $0 \leq \eta \leq 100$ mV range in 0.5 M H_2SO_4 saturated with H_2 (g).[65] In that study, η values up to 20 mV were required to generate an anodic current; the η required to achieve anodic current due to HOR decreased with increasing Pt loading. The cathodic current observed at $\eta < 20$ mV was not attributed to any particular reaction; however, the authors speculated that the adsorption of hydrogen in the first step of the HOR was inhibited at low Pt loading values, thus preventing the HOR from occurring at the standard potential.[65]

Figure 7B shows j_{HOR} values obtained at $E = 0.150$ V for the Pt/Ni foams with various values of the $A_{ecsa,Pt}/A_{ecsa,total}$ ratio, as well as for the unmodified Ni foam and Pt(poly). The j_{HOR} value for the unmodified Ni foam is marked with a green line and serves as a reference; this value is very close to zero. The j_{HOR} value for Pt(poly) is marked as a blue line and also acts as a reference. The black circles represent the j_{HOR} values obtained when I is divided by $A_{ecsa,total}$. In this case, the Ni foam is considered to contribute toward HOR, but in reality its contribution is negligible; therefore, the surface area of Ni foam should not be included in j_{HOR} determination. The red triangles represent the j_{HOR} values obtained when I is divided by $A_{ecsa,Pt}$. In this case, the Ni foam is considered inactive toward HOR and merely serves as a support for the Pt particles. As expected, such calculated j_{HOR} values are higher because $A_{ecsa,Pt}$ is significantly smaller than $A_{ecsa,total}$. Figure 7B also demonstrates that there is a correlation between the values of $A_{ecsa,Pt}$ and j_{HOR}. The Pt/Ni foams with higher $A_{ecsa,Pt}/A_{ecsa,total}$ ratios produce high j_{HOR} values, as expected. Because the performance of the Pt/Ni foams as electrocatalysts for HOR is rather poor, the analysis of these materials as electrocatalysts for HOR is not extended to include the Tafel polarization curves.

The Oxygen Reduction Reaction. Figure 8A displays LSV profiles for ORR taking place at the unmodified Ni foam, Pt(poly), and three Pt/Ni foams with various $A_{ecsa,Pt}$ values. The LSV profiles were acquired in the $1.10 \leq E \leq 0.60$ V range, in 0.50 M aqueous KOH saturated with O_2 (g), at $T = 293$ K, and $s = 0.1$ mV s^{-1}. Typical studies of ORR are carried out using a rotating disk electrode to increase the mass transport of O_2 (g) toward the electrode. The ORR experiments presented herein were carried out in lightly stirred electrolyte with a stationary electrode. We wish to add that the unmodified Ni foam and Pt/Ni foams are prepared by attaching the foam material to a thin Ni wire for electrical contact. Because of this

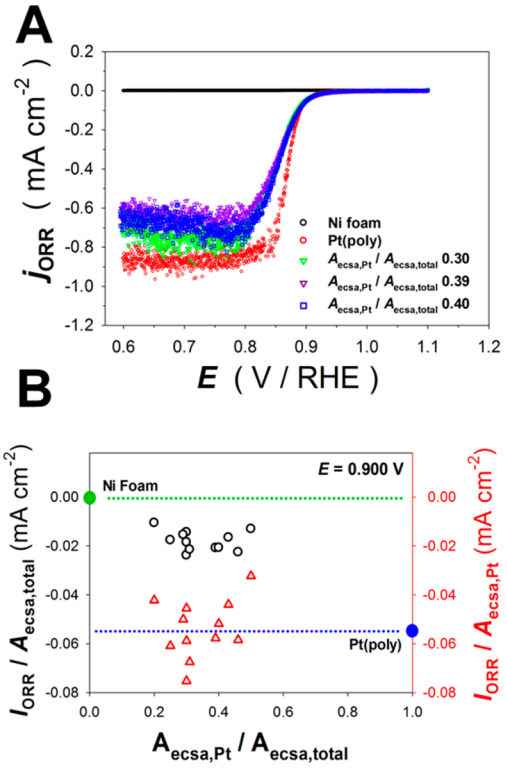

Figure 8. (A) Linear sweep voltammetry (LSV) profiles for the oxygen reduction reaction (ORR) in 0.50 M KOH using the following electrodes: Ni foam (black); Pt(poly) (red); and Pt/Ni foams with different $A_{ecsa,Pt}/A_{ecsa,total}$ ratio values: 0.30 (green), 0.39 (purple), 0.40 (blue); $s = 0.1$ mV s^{-1}, $T = 293$ K. (B) ORR current density (j_{ORR}) values at $E = 0.900$ V for Pt(poly), Ni foam, and Pt/Ni foam electrodes with various $A_{ecsa,Pt}/A_{ecsa,total}$ ratio; these values are obtained from LSV profiles. Black circles correspond to j_{HER} values normalized to $A_{ecsa,total}$; red triangles correspond to j_{HER} values normalized to $A_{ecsa,Pt}$.

arrangement the electrode cannot be rotated. The electrolyte solution cannot be agitated vigorously because this would loosen the Ni foam−Ni wire connection. Also, the reactant gas (here O_2) cannot be bubbled vigorously because this could also loosen the Ni foam−Ni wire connection. Therefore, all experiments were conducted with the electrolyte being presaturated with O_2 (g), the reactant gas passed above the electrolyte surface to maintain saturation, and the electrolyte being lightly stirred. The LSV profile for the unmodified Ni foam demonstrates that this material has practically no electrocatalytic activity toward ORR. Generally, the ORR proceeds toward the formation of hydrogen peroxide with low current density using a polycrystalline Ni electrode; however, the oxidation state of the electrode surface has a significant effect on this reaction.[66,67] The presence of electrochemically formed surface oxides on Ni was shown to inhibit the ORR.[67] The LSV ORR experiments presented herein begin at a potential ($E = 1.10$ V) well within the region of nickel oxide formation. Therefore, the presence of β-Ni(OH)$_2$ covering the Ni foam substrate is likely the reason for its inactivity toward the ORR. As expected, the LSV profile for Pt(poly) reveals that it is an active electrocatalyst toward ORR. The LSV profiles corresponding to the Pt/Ni foams display electrocatalytic behavior similar to that of Pt(poly) but with lower j_{ORR} values. It is important to emphasize that because the unmodified Ni foam displays no electrocatalytic activity toward ORR, the LSV

profiles for the Pt/Ni foams are normalized by dividing I by the $A_{ecsa,Pt}$. All of the LSV profiles display a scatter of j_{ORR} values for $E \leq 0.85$ V. This behavior is assigned to mass transport phenomena because in the case of a lightly stirred electrolyte there is nonuniform O_2 (g) concentration distribution and slow O_2 (g) diffusion from the surface region that is saturated with O_2 (g).[53] The LSV profiles for ORR on Pt(poly) and the Pt/Ni foams display similar features. Although $E°$ for ORR is 1.229 V, a large overpotential is required to achieve an appreciable current density because $j_{o,ORR}$ is several orders of magnitude lower than $j_{o,HER}$.[53] Here, an appreciable j_{ORR} value is observed only at $E < 0.93$ V. As the E decreases, the values of j_{ORR} increase and reach a maximum at ca. $E = 0.8$ V. At potential lower than 0.8 V, ORR becomes limited by the mass transport, and the value of j_{ORR} decreases with respect to the maximum value because the Nernst diffusion layer increases in thickness.

There are some notable differences between the behavior of Pt(poly) and the Pt/Ni foams that are evident from Figure 8A: (i) the increase in j_{ORR} with decreasing E is steeper for Pt(poly) than it is for the Pt/Ni foams; (ii) the influence of mass-transfer limitation is observed at a higher E value for Pt(poly) than it is for the Pt/Ni foams; this can be easily explained bearing in mind that in the case of Pt(poly) the diffusion of O_2 (g) toward the electrode can be treated as planar and, in the case of Pt particles on a Ni substrate, as hemispherical (as discussed above for HOR); and (iii) the j_{ORR} values achieved at $E < 0.80$ V (mass transport limited j) are higher for Pt(poly) than they are for the Pt/Ni foams. In the case of Pt(poly), there are two processes that occur concurrently within the E region of the ORR: the formation of PtO in the $0.85 \leq E \leq 1.23$ V range and the reduction of PtO at $0.50 \leq E \leq 1.10$ V. At the nearly steady-state conditions of this LSV experiment, the contributions of j from PtO formation and reduction are negligible. In the case of Pt/Ni foams, the PtO formation and reduction reactions occur as well. However, the formation of β-$Ni(OH)_2$ also occurs in this E region and has a greater implication for the ORR behavior of Pt/Ni foams. The formation of β-$Ni(OH)_2$ gives rise to an anodic current at $E > 0.50$ V that adds to the cathodic current of ORR. This could be the reason why the steep, linear part of the j_{ORR} versus E transients ($0.82 \leq E \leq 0.89$ V range) for the Pt/Ni foams have lower slope than the analogous transient for Pt(poly). The high surface area and porous structure of the Pt/Ni foams is another reason why these materials display lower j_{ORR} values as compared to Pt(poly). Basically, the diffusion of O_2 (g) within a network of interconnected pores is slower than it is in the case of smooth electrode. In addition, the interconnected pores also increase the IR drop, and thus the potential experienced by an inner portion of foam is lower than the actual applied potential. Finally, a growing β-$Ni(OH)_2$ layer adjacent to a Pt particle gradually decreases the latter's surface area at its edge.

Figure 8B shows the j_{ORR} values obtained at $E = 0.900$ V for the Pt/Ni foam electrodes with various values of the $A_{ecsa,Pt}/A_{ecsa,total}$ ratio, as well as for the unmodified Ni foam and Pt(poly). The j_{ORR} value for the unmodified Ni foam is marked with a green line and serves as a reference. As is the case with HOR, the activity of Ni foam toward ORR is below 0.1 μA cm^{-2} that in this graph is very close to zero. The j_{ORR} value for Pt(poly) is marked as a blue line and also acts as a reference. The black circles represent the j_{ORR} values obtained when I is divided by the $A_{ecsa,total}$. In this case, the Ni foam is considered to contribute toward ORR, but in reality its contribution is negligible; therefore, the surface area of Ni foam should not be included in the j_{ORR} determination. The red triangles represent the j_{ORR} values obtained when I is divided by $A_{ecsa,Pt}$. In this case, the Ni foam is considered inactive toward ORR and merely serves as a support for the Pt particles. As expected, such calculated j_{ORR} values are higher because $A_{ecsa,Pt}$ is significantly smaller than $A_{ecsa,total}$. Figure 8B also demonstrates that although the j_{ORR} values reveal a scatter, they are centered around the j_{ORR} value for Pt(poly). Since the electrocatalytic behavior of the Pt/Ni foams is similar to that of Pt(poly), the analysis of these materials for ORR is not extended to include the Tafel polarization curves.

The Oxygen Evolution Reaction. Figure 9A shows LSV profiles for OER taking place at the unmodified Ni foam, Pt(poly), and three Pt/Ni foams with various $A_{ecsa,Pt}$ values. The LSV profiles were collected in the $1.35 \leq E \leq 1.80$ V region, in 0.50 M aqueous KOH electrolyte saturated with O_2 (g), at $T = 293$ K, and $s = 0.1$ mV s^{-1}; the electrolyte was lightly stirred during the measurement. The analysis of OER taking place at the Pt/Ni foams differs slightly from those for HER, HOR, and ORR because Ni materials are known to be more effective electrocatalysts toward this reaction than Pt(poly).[68] In this case, the performance of Pt/Ni foams is examined to determine if there are any electrocatalytic benefits associated with depositing Pt on Ni foam. The current density for OER (j_{OER}) taking place at the unmodified Ni foam is significantly higher than that for Pt(poly), thus indicating that despite its noble character platinum is not a good electrocatalyst for this reaction in an alkaline medium. The Pt/Ni foams yield j_{OER} values that are intermediate as compared to the analogous values for the unmodified Ni foam and Pt(poly). The LSV profiles demonstrate an increase in the electrocatalytic activity with decreasing value of the $A_{ecsa,Pt}/A_{ecsa,total}$ ratio. This is attributed to the presence of Pt particles physically blocking regions of the underlying Ni, thus reducing its surface area. Figure 9A demonstrates that among all the materials studied, the unmodified Ni foam reveals the highest j_{OER} values over practically the entire E range employed and the lowest activation overpotential. Large η values are typically required for OER to proceed regardless of the electrocatalyst material.[53] Since both Ni and Pt are electrocatalytically active toward OER, j_{OER} is determined by dividing I by $A_{ecsa,total}$.

Figure 9B shows the j_{OER} values obtained at $E = 1.65$ V for the Pt/Ni foam electrodes, as well as for the unmodified Ni foam and Pt(poly). These values were obtained from the LSV profiles and are plotted as a function of $A_{ecsa,Pt}/A_{ecsa,total}$. The j_{OER} values for the unmodified Ni foam and Pt(poly) are shown as green and blue circles, respectively. To facilitate a comparative data analysis, we add dotted horizontal lines that represent the j_{OER} values for the untreated Ni foam and Pt(poly). The black circles represent the j_{OER} values obtained when I is divided by $A_{ecsa,total}$. In this case, both the deposited Pt and the underlying Ni foam act as electrocatalytic materials at which OER takes place. The purple triangles represent the j_{OER} values obtained when I is divided by only $A_{ecsa,Ni}$. In this case, the Pt particles are considered electrocatalytically inactive, and the entire I for OER is attributed to the Ni foam. In all cases, the j_{OER} values obtained when I is divided by $A_{ecsa,Ni}$ (the purple triangles) are greater than when I is divided by $A_{ecsa,total}$ (the black circles). We also observe that the black circles and purple triangles overlap because Pt is electrocatalytically active toward OER although less than Ni. The purple triangles reveal a scatter and are above and below the j_{OER} value for the unmodified Ni. The scatter could be attributed to the experimental uncertainty

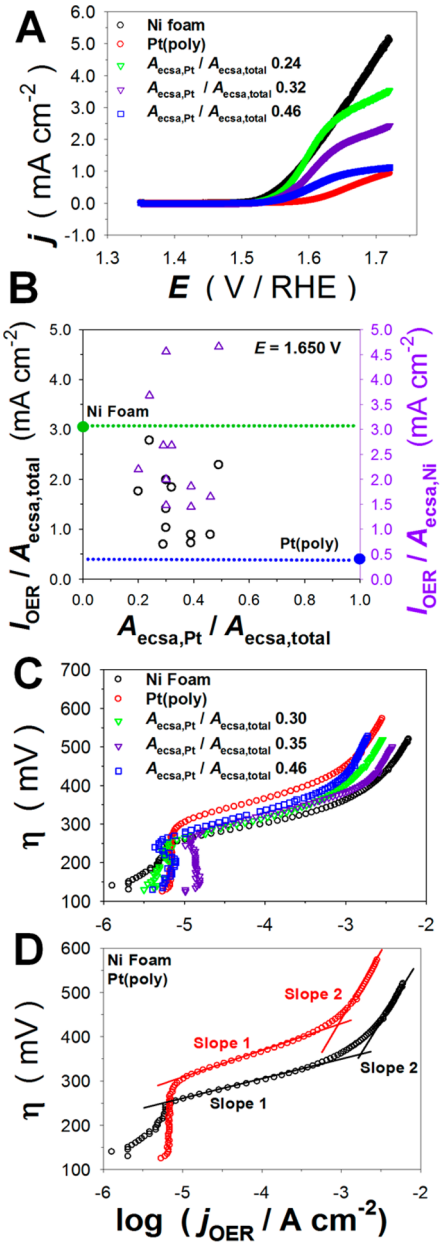

Figure 9. (A) Linear sweep voltammetry (LSV) profiles for the oxygen evolution reaction (OER) in 0.50 M KOH using the following electrodes: Ni foam (black); Pt(poly) (red); and Pt/Ni foams with different $A_{ecsa,Pt}/A_{ecsa,total}$ ratio values: 0.24 (green), 0.32 (purple), 0.46 (blue); s = 0.1 mV s^{-1}, T = 293 K. (B) OER current density (j_{OER}) values at E = 1.650 V for Pt(poly), Ni foam, and Pt/Ni foam electrodes with various $A_{ecsa,Pt}/A_{ecsa,total}$ ratios; these values are obtained from LSV profiles. Black circles correspond to j_{OER} values normalized to $A_{ecsa,total}$; purple triangles correspond to j_{OER} values normalized to the electrochemical surface area of Ni $A_{ecsa,Ni}$. (C) OER Tafel polarization plots for unmodified Ni foam (black), Pt(poly) (red), and Pt/Ni foam electrodes with various $A_{ecsa,Pt}/A_{ecsa,total}$ ratios: 0.30 (green), 0.35 (purple), 0.46 (blue) carried out in 0.50 M KOH at T = 293 K. (D) Illustration for the determination of the Tafel slope (b) and exchange current density ($j_{o,OER}$) from Tafel polarization curves of Pt(poly) and unmodified Ni foam electrodes.

associated with the determination of $A_{ecsa,Ni}$ of Ni foams that is ca. 30%, as explained elsewhere.[44] However, it is interesting to observe that an average of all the points would fall slightly below the j_{OER} value for Ni foam.

Figure 9C presents Tafel polarization plots for OER taking place on the unmodified Ni foam, Pt(poly), and three Pt/Ni foams with different values of $A_{ecsa,Pt}$. The Tafel plots for Pt(poly) and the Pt/Ni foam electrodes display similar features over the entire overpotential range. At η < 250 mV, the slope is very high and has an unusual shape; this region corresponds to the part of the LSV profile where no appreciable j_{OER} is observed, that is, to the region of activation overpotential. There is an intermediate η linear region where the Tafel slope is low (the slope 1 in Figure 9D), and there is a high η linear region where the slope is high (the slope 2 in Figure 9D). The Tafel polarization plot for the unmodified Ni foam is similar to those for the Pt/Ni foams and Pt(poly). In the case of Ni foam, the low η region reveals a moderate slope, which is attributed to the formation of β-NiOOH in the 1.20 ≤ E ≤ 1.55 V range occurring concurrently with OER and affecting its rate. Figure 9D shows Tafel plots for Pt(poly) and the unmodified Ni foam to clearly demonstrate the two linear regions described above.

Table 1 presents the exchange current density ($j_{o,OER}$) and Tafel slope (b) values obtained for each type of material and facilitates a comparative analysis of their electrocatalytic activity. There are two linear regions for the unmodified Ni foam, Pt(poly), and Pt/Ni foams; thus, there are two sets of $j_{o,OER}$ and b values. Although the j_{OER} values are of the same order of magnitude, the b value at low overpotentials for the unmodified Ni foam is significantly lower than those for Pt(poly) and the Pt/Ni foams.

CONCLUSIONS

The results presented in this paper contribute to the understanding of Ni foams as electrocatalysts and as support materials for Pt nanoparticles; the latter can be prepared on Ni foam substrates via electroless deposition. The Pt nanoparticles are deposited through the reduction of Pt^{2+} or Pt^{4+} cations using an aqueous $NaBH_4$ solution as a reducing agent. The values of $A_{ecsa,Pt}$ and m_{Pt} can be tailored by controlling the type and concentration of Pt cations in the deposition solution and by selecting the number of deposition events. The values of $A_{ecsa,Pt}$ can be related to the values of m_{Pt}; their ratio sheds light on the size of Pt nanoparticles, their agglomeration, and the Pt mass enhancement factor. The values of $A_{ecsa,Pt}/m_{Ni}$ and m_{Pt}/m_{Ni} are in the 40−300 cm^2 g^{-1} and 250−2200 μg g^{-1} ranges, respectively. An SEM analysis of the morphology and size of the Pt deposit demonstrates that the Pt particles have circular shapes with dimensions in the 5−30 nm range. A correlation of SEM and EDS results indicate that the surfaces of Pt/Ni foam struts are covered uniformly with the Pt nanoparticles. The electrochemical stability of the Pt/Ni foams is examined upon prolonged potential cycling by evaluating qualitative changes in the CV profiles and the values of $A_{ecsa,total}$, I_{DL}, Q_{anodic}, and $Q_{cathodic}$ as a function of cycle number. The potential cycling results in a reduction in j of all the CV features and points to a decrease of $A_{ecsa,Pt}$ that may be attributed to the following phenomena: (i) detachment of Pt nanoparticles; (ii) electrodissolution of Pt nanoparticles; (iii) electrodeposition of Pt on existing nanoparticles resulting in an increase of their size; and (iv) surface morphology change of Pt nanoparticles via oxide formation and reduction leading to a lower roughness. The oxidation state of Pt (Pt^{2+} versus Pt^{4+}) in the salt used to produce Pt nanoparticles, the salt concentration, and the number of deposition events determine the values of $A_{ecsa,Pt}/m_{Ni}$ and m_{Pt}/m_{Ni} as well as the size and distribution of Pt nanoparticles.

The electrocatalytic activity of the unmodified Ni foam, the Pt/Ni foams, and Pt(poly) toward HER, HOR, ORR, and OER in alkaline media is examined using LSV profiles and steady-state Tafel polarization plots. In the case of HER, Pt(poly) is the most active electrocatalyst, followed by the Pt/Ni foams, and the unmodified Ni foam. The Pt/Ni foams reveal a synergetic effect in the sense that j_{HER} for the Pt/Ni foams is higher than that for Pt(poly). In the case of HOR, the unmodified Ni foams and Pt/Ni foams are poor electrocatalysts, and the latter generate small anodic j_{HOR} only at large η values. In the case of ORR, the unmodified Ni foam displays no electrocatalytic activity. The Pt/Ni foams and Pt(poly) reveal good electrocatalytic activity; the activity of Pt/Ni foams correlates with $A_{ecsa,Pt}$ indicating that the Ni foam acts as an electronically conducting support and that there is no synergetic effect. In the case of OER, the unmodified Ni foam is a good electrocatalyst, and the Pt/Ni foams and Pt(poly) display moderate electrocatalytic activity. The Pt nanoparticles on the Ni substrate do not produce any synergetic effect and reduce j_{OER} by reducing $A_{ecsa,Ni}$.

Deposition of Pt nanoparticles on Ni foams can be achieved in a reproducible manner using an electroless deposition method. Such prepared Pt/Ni foams are promising materials for HER. These materials are also applicable to ORR because the electrocatalytic activity of Pt and the nanostructure of the deposit are preserved, while the Ni foam offers an extended solid−liquid interface. The Pt/Ni foams are not good electrocatalysts for HOR. The unmodified Ni foam is an excellent electrocatalyst for OER, and the deposition of Pt nanoparticles has no synergetic effect and only reduces $A_{ecsa,Ni}$. In summary, Ni foams are relatively new materials that reveal new and promising electrocatalytic properties. Although this research is dedicated to their modification with Pt nanoparticles, it calls for further research on their modification with other materials known to possess good catalytic properties.

■ ASSOCIATED CONTENT

Supporting Information

This file provides more detailed information regarding certain experimental procedures and additional information on the three-dimensional structure of nickel foam. This material is available free of charge via the Internet at http://pubs.acs.org.

■ AUTHOR INFORMATION

Corresponding Author

*E-mail: Gregory.jerkiewicz@chem.queensu.ca.

Author Contributions

The manuscript was written through contributions of all authors. All authors have given approval to the final version of the manuscript.

Notes

The authors declare no competing financial interest.

■ ACKNOWLEDGMENTS

The authors gratefully acknowledge financial support towards this project from the Natural Science and Engineering Research Council of Canada (Discovery, Strategic and Equipment Grants), the Canada Foundation for Innovation (Infrastructure Project at Queen's University), and the Canada Research Chairs Program (B.D. Gates). This work made use of 4D LABS shared facilities supported by the Canada Foundation for Innovation (CFI), British Columbia Knowledge Development Fund (BCKDF), Western Economic Diversification Canada, and Simon Fraser University. They also acknowledge support from Vale (formerly Vale-Inco) and discussions with their personnel, Drs. V. Paserin and Q. Yang.

■ ABBREVIATIONS

A_{ecsa}, electrochemical surface area
A_s, specific surface area
b, Tafel slope
C_{DL}, double-layer capacitance
CE, counter electrode
CV, cyclic voltammetry
E, potential
EDS, energy dispersive X-ray spectroscopy
EIS, electrochemical impedance spectrometry
FIB, focused ion beam
HER, hydrogen evolution reaction
HOR, hydrogen oxidation reaction
H_{UPD}, under potential deposition of hydrogen
I, current
I_{DL}, double layer current
ICP−OES, inductively coupled plasma optical emission spectroscopy
j, current density
j°, exchange current density
j_{HER}, current density of the hydrogen evolution reaction
j_{HOR}, current density of the hydrogen oxidation reaction
j_{ORR}, current density of the oxygen reduction reaction
j_{OER}, current density of the oxygen evolution reaction
LSV, linear sweep voltammetry
OER, oxygen evolution reaction
ORR, oxygen reduction reaction
Pt_{poly}, polycrystalline platinum
Q, charge
Q_{anodic}, anodic charge
$Q_{cathodic}$, cathodic charge
RE, reference electrode
RHE, reversible hydrogen electrode
RΩ, uncompensated solution resistance
s, scan rate
SEM, scanning electron microscopy
T, temperature
UHP, ultrahigh purity
WE, working electrode
3D, three-dimensional
η, overpotential
ρ, bulk density

■ REFERENCES

(1) Naterer, G. F.; Fowler, M.; Cotton, J.; Gabriel, K. Synergistic Roles of Off-Peak Electrolysis and Thermochemical Production of Hydrogen from Nuclear Energy in Canada. *Int. J. Hydrogen Energy* **2008**, *33*, 6849−6857.

(2) Zeng, K.; Zhang, D. Recent Progress in Alkaline Water Electrolysis for Hydrogen Production and Applications. *Prog. Energy Combust. Sci.* **2010**, *36*, 307−326.

(3) Carmo, H.; Fritz, D. L.; Mergel, J. S. A Comparative Review on PEM Water Electrolysis. *Int. J. Hydrogen Energy* **2013**, *38*, 4901−4934.

(4) Divisek, J. Determination of the Kinetic of Hydrogen Evolution by Analysis of the Potential−Current and Potential−Coverage Curves. *J. Electroanal. Chem.* **1986**, *214*, 615−632.

(5) Harrington, D.; Conway, B. E. Kinetic Theory of the Open−Circuit Potential Decay Method for the Evaluation of Behaviour of

Adsorbed Intermediates; Analysis for the Case of the H_2 Evolution Reaction. *J. Electroanal. Chem.* **1987**, *221*, 1−12.
(6) Lasia, A.; Rami, A. Kinetics of Hydrogen Evolution on Nickel Electrodes. *J. Electroanal. Chem.* **1990**, *294*, 123.
(7) Chen, L.; Lasia, A. Study of the Kinetics of Hydrogen Evolution Reaction on Nickel−Zinc Alloy Electrodes. *J. Electrochem. Soc.* **1991**, *138*, 3321−3328.
(8) Machado, S. A. S.; Avaca, L. A. The Hydrogen Evolution Reaction on Nickel Surfaces Stabilized by H-Absorption. *Electrochim. Acta* **1994**, *39*, 1385.
(9) Krstajic, N.; Popovic, K. D.; Grgur, B. N.; Vojnovic, M.; Sepa, D. On the Kinetics of the Hydrogen Evolution Reaction on Nickel in Alkaline Solution. *J. Electroanal. Chem.* **2001**, *512*, 16−26.
(10) Marini, S.; Salvi, P.; Nelli, P.; Presenti, R.; Villa, M.; Berrettoni, M.; Zangari, G.; Kiros, Y. Advanced Alkaline Water Electrolysis. *Electrochim. Acta* **2012**, *82*, 384−391.
(11) Hall, D. E. Alkaline Water Electrolysis Anode Materials. *J. Electrochem. Soc.* **1985**, *132*, 42C−48C.
(12) Floner, D. L.; Leger, J.-M. Electrocatalytic Oxidation of Hydrogen on Polycrystal and Single-Crystal Nickel Electrodes. *Surf. Sci.* **1990**, *243*, 87−97.
(13) Miles, M. H.; Huang, Y. H. The Oxygen Electrode Reaction in Alkaline Solutions on Oxide Electrodes Prepared be the Thermal Decomposition Method. *J. Electrochem. Soc.* **1978**, *125*, 1930−1933.
(14) de Carvalho, J.; Tremiliosi-Filho, G.; Avaca, L. A.; Gonzalez, E. R. Electrodeposits of Iron and Nickel−Iron for Hydrogen Evolution in Alkaline Solutions. *Int. J. Hydrogen Energy* **1989**, *14*, 161−165.
(15) Gonzalez, E. R.; de Giz, M. J. The Hydrogen Evolution Reaction on Nickel Based Electrodeposits. *Hem. Ind.* **2000**, *54*, 123−132.
(16) Rosalbino, F.; Scavino, G.; Grande, M. A. Electrocatalytic Activity of Ni−Fe−M (M = Cr, Mn, Cu) Sintered Electrodes for Hydrogen Evolution Reaction in Alkaline Solution. *J. Electroanal. Chem.* **2013**, *694*, 114−121.
(17) de Giz, M. J.; Tremiliosi-Filho, G.; Gonzalez, E. R.; Srinivasan, S.; Appleby, A. J. The Hydrogen Evolution Reaction on Amorphous Nickel and Cobalt Alloys. *Int. J. Hydrogen Energy* **1995**, *20*, 423−427.
(18) Simpraga, R.; Conway, B. E. Real Area and Electrocatalysis Factors in Hydrogen Evolution Kinetics at Electrodeposited Ni−Mo and Ni−Mo−Cd Composites: Effect of Cd Content and Nature of Substrate. *J. Appl. Electrochem.* **1995**, *25*, 628−641.
(19) Assuncao, N. A.; de Giz, M. J.; Tremiliosi-Filho, G.; Conzalez, E. R. A Study of the Hydrogen Evolution Reaction on a Ni/NiFeS Electrodeposited Coating. *J. Electrochem. Soc.* **1997**, *144*, 2794−2800.
(20) Singh, R. N.; Mishra, D.; Anindita, A.; Sinha, A. S. K.; Singh, A. Novel Electrocatalysts for Generating Oxygen from Alkaline Water Electrolysis. *Electrochem. Commun.* **2007**, *9*, 1369−1373.
(21) Song, S.; Maragou, V.; Tsiakaras, P. How Far Are Direct Alcohol Fuel Cells From Our Energy Future? *J. Fuel Cell Sci. Technol.* **2007**, *4*, 203−209.
(22) Santos, D. M. F.; Sequeira, C. A. C.; Maccio, D.; Saccone, A.; Figueiredo, J. L. Platinum−Rare Earth Electrodes for Hydrogen Evolution in Alkaline Water Electrolysis. *Int. J. Hydrogen Energy* **2013**, *38*, 3137−3145.
(23) Friedl, J.; Stimming, U. Model Catalyst Studies on Hydrogen and Ethanol Oxidation for Fuel Cells. *Electrochim. Acta* **2013**, *101*, 41−58.
(24) Ma, J.; Choudhury, N. A.; Sahai, Y. A Comprehensive Review of Direct Borohydride Fuel Cells. *Renewable Sustainable Energy Rev.* **2010**, *14*, 183−199.
(25) Yu, E. H.; Krewer, U.; Scott, K. Principles and Materials Aspects of Direct Alkaline Alcohol Fuel Cells. *Energies* **2010**, *3*, 1499−1528.
(26) Šljukić, B.; Santos, D. M. F.; Sequeira, C. A. C. Manganese Dioxide Electrocatalysts for Borohydride Fuel Cell Cathodes? *J. Electroanal. Chem.* **2013**, *694*, 77−83.
(27) Banhart, J. Manufacture, Characterization, and Application of Cellular Metals and Metal Foams. *Prog. Mater. Sci.* **2001**, *46*, 559−632.
(28) Francis, S. A.; Bergens, S. H. Low Pt-Loading Ni−Pt and Pt Deposits on Ni: Preparation, Activity, and Investigation of Electronic Properties. *J. Power Sources* **2011**, *196*, 7470−7480.
(29) Cimino, S.; Lisi, L.; Mancino, G.; Musiani, M.; Vázquez-Gómez, L.; Verlato, E. Catalytic Partial Oxidation of CH_4−H_2 Mixtures Over Ni Foams Modified with Rh and Pt. *Int. J. Hydrogen Energy* **2012**, *37*, 17040−7051.
(30) Fiameni, S.; Herraiz-Cardona, I.; Musiani, M.; Pérez-Herranz, V.; Vázquez-Gómez, L.; Verlato, E. The HER in Alkaline Media on Pt-Modified Three-Dimensional Ni Cathodes. *Int. J. Hydrogen Energy* **2012**, *37*, 10507−10516.
(31) Verlato, E.; Cattarin, S.; Comisso, N.; Mattarozzi, L.; Musiani, M.; Vazquez-Gomez, L. Reduction of Nitrate Ions at Rh−Modified Ni Foam Electrodes. *Electrocatalysis* **2013**, *4*, 203−211.
(32) Verlato, E.; Cattarin, S.; Comisso, N.; Gambirasi, A.; Musiani, M.; Vazquez-Gomez, L. Preparation of Pd-Modified Ni Foam Electrodes and Their Use as Anodeas for the Oxidation of Alcohols in Basic Media. *Electrocatalysis* **2012**, *3*, 48−58.
(33) Yang, B.; Yu, G.; Shuai, D. Electrocatalytic Hydrodechlorination of 4-Chlorobiphenyl in Aqueous Solution Using Palladized Nickel Foam Cathode. *Chemosphere* **2007**, *67*, 1361−1367.
(34) Cheng, Y.; Liu, Y.; Cao, D.; Wang, G.; Gao, Y. Effects of Acetone on Electrooxidation of 2−Propanol in Alkaline Medium on the Pd/Ni−Foam Electrode. *J. Power Sources* **2011**, *196*, 3124−3128.
(35) Chen, J.; Zhao, C. X.; Zhi, M. M.; Wang, K.; Deng, L.; Xu, G. Alkaline Direct Oxidation Glucose Fuel Cell System Using Silver/Nickel Foam as Electrodes. *Electrochim. Acta* **2012**, *66*, 133−138.
(36) Yang, C.; Zhang, D.; Zhao, Y.; Lu, Y.; Wang, L.; Goodenough, J. B. Nickel Foam Supported Sn−Co Alloy Film as Anode for Lithium Ion Batteries. *J. Power Sources* **2011**, *196*, 10673−10678.
(37) Dai, H.; Liang, Y.; Wang, P.; Yao, X.; Rufford, T.; Lu, M.; Cheng, H. High-Performance Cobalt−Tungsten−Boron Catalyst Supported on Ni Foam for Hydrogen Generation from Alkaline Sodium Borohydride Solution. *Int. J. Hydrogen Energy* **2008**, *33*, 4405−4412.
(38) Paserin, V.; Marcuson, S.; Shu, J.; Wilkinson, D. S. CVD Technique for Inco Nickel Foam Production. *Adv. Eng. Mater.* **2004**, *6*, 454−459.
(39) Ostgard, D.; Kustov, L.; Poeppelmeier, K.; Sachtler, W. Comparison of Pt/KL Catalysts Prepared by Ion Exchange or Incipient Wetness Impregnation. *J. Catal.* **1992**, *133*, 342−357.
(40) Antolini, E.; Salgado, J.; Dos Santos, A.; Gonzalez, E. Carbon-Supported Pt−Ni Alloys Prepared by the Borohydride Method as Electrocatalysts for DMFCs. *Electrochem. Solid-State Lett.* **2005**, *8*, A226−A230.
(41) Esmaeilifar, A.; Rowshanzamir, S.; Eikani, M. H.; Ghazanfari, E. Preparation of Low-Platinum-Loading Electrocatalysis Using Electroless Deposition Method for Proton Exchange Membrane Fuel Cell Systems. *Electrochim. Acta* **2010**, *56*, 271−277.
(42) Rooke, J.; de Matos Passos, C.; Chatenet, M.; Sescousse, R.; Budtova, T.; Berthon-Fabry, S.; Mosdale, R.; Maillard, F. Synthesis and Properties of Platinum Nanocatalyst Supported on Cellulose-Based Carbon Aerogel for Applications in PEMFCs. *J. Electrochem. Soc.* **2011**, *158*, B779−B789.
(43) Veizaga, N.; Fernandez, J.; Bruno, M.; Scelza, O.; de Miguel, S. Deposition of Pt Nanoparticles on Different Carbonaceous Materials by Using Different Preparation Methods for PEMFC Electrocatalysts. *Int. J. Hydrogen Energy* **2012**, *37*, 17910−17920.
(44) Grden, M.; Alsabet, M.; Jerkiewicz, G. Surface Science and Electrochemical Analysis of Nickel Foams. *ACS Appl. Mater. Interfaces* **2012**, *4*, 3012−3021.
(45) van Drunen, J.; Kinkead, B.; Wang, M. C. P.; Gates, B. D.; Sourty, E.; Jerkiewicz, G. Comprehensive Structural, Surface-Chemical and Electrochemical Characterization of Nickel-Based Metallic Foams. *ACS Appl. Mater. Interfaces* **2013**, *5*, 6712−6722.
(46) Angerstein-Kozlowska, H. In *Comprehensive Treatise of Electrochemistry Vol. 9;* Yeager, E., Ed.; Plenum Press: New York, 1984; pp 15−58.
(47) Hall, D. S.; Bock, C.; MacDougall, B. R. Surface Layers in Alkaline Media: Nickel Hydrides on Metallic Nickel Electrodes. *J. Electrochem. Soc.* **2013**, *160*, F235−F243.

(48) Stevie, F. A.; Giannuzzi, L. A.; Prenitzer, B. I.; In *Introduction to Focused Ion Beams Instrumentation, Theory, Techniques and Practice;* Giannuzzi, L. A., Stevie, F. A., Eds.; Springer: New York, NY, 2005; p 1−12.
(49) Furuya, N.; Shibata, M. Structural Changes at Various Ot Single Crystal Surfaces with Potential Cycles in Acidic and Alkaline Solutions. *J. Electroanal. Chem.* **1999**, *467*, 85−91.
(50) Schmidt, T. J.; Ross, P. N.; Markovic, N. M. Temperature Dependent Surface Electrochemistry on Pt Single Crystals in Alkaline Electrolytes, Part 2. The Hydrogen Evolution/Oxidation Reaction. *J. Electroanal. Chem.* **2002**, *524*, 252−260.
(51) Trasatti, S.; Petrii, O. A. Real Surface Area Measurements in Electrochemistry. *J. Electroanal. Chem.* **1992**, *327*, 353−376.
(52) Chen, D.; Tao, Q.; Liao, L. W.; Liu, S. X.; Chen, Y. X.; Ye, S. Determining the Active Surface Area for Various Platinum Electrodes. *Electrocatalysis* **2011**, *2*, 20−219.
(53) Hamann, C. H.; Hamnett, A.; Vielstich, W. *Electrochemistry;* Wiley-VCH: Darmstadt, Germany, 2007.
(54) Kinkead, B.; van Drunen, J.; Paul, M. Y. T.; Dowling, K.; Jerkiewicz, G.; Gates, B. D. Platinum Ordered Porous Electrodes: Developing a Platform for Fundamental Electrochemical Characterization. *Electrocatalysis* **2013**, *4*, 179−186.
(55) Kim, S.; Meyers, J. P. The Influence of Hydrogen- and Cation-Underpotential Deposition on Oxide-Mediated Pt Dissolution in Proton-Exchange Membrane Fuel Cells. *Electrochim. Acta* **2011**, *56*, 8387−8393.
(56) Xing, L.; Jerkiewicz, C.; Beauchemin, D. Ion Exchange Chromatography Coupled to Inductively Coupled Plasma Mass Spectrometry for the Study of Pt Electro−Dissolution. *Anal. Chim. Acta* **2013**, *785*, 16−21.
(57) Topalov, A. A.; Katsounaros, I.; Auinger, M.; Cerevko, S.; Meier, J. C.; Klemm, S. O.; Mayrhofer, K. J. J. Dissolution of Platinum: Limits for the Deployment of Electrochemical Energy Conversion? *Angew. Chem., Int. Ed.* **2012**, *51*, 1−4.
(58) Holzwarth, U.; Gibson, N. The Scherrer Equation Versus the 'Debye−Scherrer Equation'. *Nat. Nanotechnol.* **2011**, *6*, 534−538.
(59) Trasatti, S. Work Function, Electronegativity, and Electrochemical Behaviour of Metals. III. Electrolytic Hydrogen Evolution in Acid Solutions. *J. Electroanal. Chem. Interfacial Electrochem.* **1972**, *39*, 163−184.
(60) Park, K.; Choi, J.; Kwon, N.; Lee, S.; Sung, Y.; Ha, H.; Hong, S.; Kim, H.; Wieckowski, A. Chemical and Electronic Effects of Ni in Pt/Ni and Pt/Ru/Ni Alloy Nanoparticles in Methanol Electrooxidation. *J. Phys. Chem. B* **2002**, *106*, 1869−1877.
(61) Toda, T.; Igarashi, H.; Uchida, H.; Watanabe, M. Enhancement of the Electrocatalytic O_2 Reduction on Pt−Fe Alloys. *J. Electrochem. Soc.* **1999**, *146*, 3750−3756.
(62) Tegou, A.; Papadimitriou, S.; Armyanov, S.; Valova, E.; Kokkinidis, G.; Sotiropoulos, S. Oxygen Reduction at Platinum− and Gold-Coated Iron, Cobalt, Nickel and Lead Deposits on Glassy Carbon Substrates. *J. Electroanal. Chem.* **2008**, *623*, 187−196.
(63) Martinez-Huitle, C. A.; Ferro, S.; De Battisti, A. Electrochemical Incineration of Oxalic Acid Role of Electrode Material. *Electrochim. Acta* **2004**, *49*, 4027−4034.
(64) Weininger, J. L.; Breiter, M. W. Hydrogen Evolution and Surface Oxidation of Nickel Electrodes in Alkaline Solution. *J. Electrochem. Soc.* **1964**, *111*, 707−712.
(65) Croissant, M. J.; Napporn, T.; Léger, J.-M.; Lamy, C. Electrocatalytic Oxidation of Hydrogen at Platinum-Modified Polyaniline Electrodes. *Electrochim. Acta* **1998**, *43*, 2447−2457.
(66) Bagotzky, V. S.; Shumilova, N. A.; Khrushcheva, E. I. Electrochemical Oxygen Reduction on Oxide Catalysts. *Electrochim. Acta* **1976**, *21*, 919−924.
(67) Bagotzky, V. S.; Shumilova, N. A.; Samoilov, G. P.; Khrushcheva, E. I. Electrochemical Oxygen Reduction on Nickel Electrodes in Alkaline Solutions—II. *Electrochim. Acta* **1972**, *17*, 1625−1635.
(68) Scarr, R. F. The Mechanism of Oxygen Evolution on Nickel, Platinum, and Other Metals and Alloys. *J. Electrochem. Soc.* **1969**, *116*, 1526−1532.